



HAL
open science

Localized Irradiation of Cell Membrane by Auger Electrons Is Cytotoxic Through Oxidative Stress-Mediated Nontargeted Effects

Salomé Paillas, Riad Ladjohounlou, Catherine Lozza, Alexandre Pichard, Vincent Boudousq, Marta Jarlier, Samuel Sevestre, Marion Le Blay, Emmanuel Deshayes, Jane Sosabowski, et al.

► To cite this version:

Salomé Paillas, Riad Ladjohounlou, Catherine Lozza, Alexandre Pichard, Vincent Boudousq, et al.. Localized Irradiation of Cell Membrane by Auger Electrons Is Cytotoxic Through Oxidative Stress-Mediated Nontargeted Effects. *Antioxidants and Redox Signaling*, 2016, 25 (8), pp.467 - 484. 10.1089/ars.2015.6309 . hal-01905223

HAL Id: hal-01905223

<https://hal.science/hal-01905223>

Submitted on 26 Nov 2020

HAL is a multi-disciplinary open access archive for the deposit and dissemination of scientific research documents, whether they are published or not. The documents may come from teaching and research institutions in France or abroad, or from public or private research centers.

L'archive ouverte pluridisciplinaire **HAL**, est destinée au dépôt et à la diffusion de documents scientifiques de niveau recherche, publiés ou non, émanant des établissements d'enseignement et de recherche français ou étrangers, des laboratoires publics ou privés.

ORIGINAL RESEARCH COMMUNICATION

Localized Irradiation of Cell Membrane by Auger Electrons Is Cytotoxic Through Oxidative Stress-Mediated Nontargeted Effects

Salomé Paillas,¹⁻⁵ Riad Ladjohounlou,¹⁻⁴ Catherine Lozza,¹⁻⁴ Alexandre Pichard,¹⁻⁴ Vincent Boudousq,¹⁻⁴ Marta Jarlier,⁴ Samuel Sevestre,¹⁻⁴ Marion Le Blay,¹⁻⁴ Emmanuel Deshayes,¹⁻⁴ Jane Sosabowski,⁵ Thierry Chardès,¹⁻⁴ Isabelle Navarro-Teulon,¹⁻⁴ Robert J Mairs,⁶ and Jean-Pierre Pouget¹⁻⁴

Abstract

Aims: We investigated whether radiation-induced nontargeted effects are involved in the cytotoxic effects of anticell surface monoclonal antibodies labeled with Auger electron emitters, such as iodine 125 (monoclonal antibodies labeled with ¹²⁵I [¹²⁵I-mAbs]). **Results:** We showed that the cytotoxicity of ¹²⁵I-mAbs targeting the cell membrane of p53^{+/+} HCT116 colon cancer cells is mainly due to nontargeted effects. Targeted and nontargeted cytotoxicities were inhibited *in vitro* following lipid raft disruption with Methyl- β -cyclodextrin (MBCD) or filipin or use of radical oxygen species scavengers. ¹²⁵I-mAb efficacy was associated with acid sphingomyelinase activation and modulated through activation of the AKT, extracellular signal-related kinase 1/2 (ERK1/2), p38 kinase, c-Jun N-terminal kinase (JNK) signaling pathways, and also of phospholipase C- γ (PLC- γ), proline-rich tyrosine kinase 2 (PYK-2), and paxillin, involved in Ca²⁺ fluxes. Moreover, the nontargeted response induced by directing 5-[(125)I]iodo-2'-deoxyuridine to the nucleus was comparable to that of ¹²⁵I-mAb against cell surface receptors. *In vivo*, we found that the statistical significance of tumor growth delay induced by ¹²⁵I-mAb was removed after MBCD treatment and observed oxidative DNA damage beyond the expected Auger electron range. These results suggest the involvement of nontargeted effects *in vivo* also. **Innovation:** Low-energy Auger electrons, such as those emitted by ¹²⁵I, have a short tissue range and are usually targeted to the nucleus to maximize their cytotoxicity. In this study, we show that targeting the cancer cell surface with ¹²⁵I-mAbs produces a lipid raft-mediated nontargeted response that compensates for the inferior efficacy of non-nuclear targeting. **Conclusion:** Our findings describe the mechanisms involved in the efficacy of ¹²⁵I-mAbs targeting the cancer cell surface. *Antioxid. Redox Signal.* 00, 000–000.

Introduction

THE HIGHLY LOCALIZED CYTOTOXICITY of Auger electrons is particularly attractive for targeted radionuclide therapy of microscopic or metastatic disease because it allows the irradiation of tumor cells while sparing healthy tissues. Auger electrons are produced in atoms decaying by

internal conversion or electron capture. These processes create a vacancy in the inner electron shell that is subsequently filled by electrons dropping in from higher energy levels. Thus, the vacancy moves to the outer shells, and the transition is accompanied by cascades of complex emissions of Auger, Coster–Kronig, and super Coster–Kronig electrons (collectively called Auger electrons) and soft X-rays [for

¹Institut de Recherche en Cancérologie de Montpellier (IRCM), Montpellier, France.

²INSERM, U1194, Montpellier, France.

³Université de Montpellier, Montpellier, France.

⁴Institut régional du Cancer de Montpellier, Montpellier, France.

⁵Barts Cancer Institute, Queen Mary University of London, London, United Kingdom.

⁶Institute of Cancer Sciences, University of Glasgow, Glasgow, Scotland.

Innovation

Because of their physical properties, Auger electron emitters, such as iodine 125 (^{125}I), are usually targeted to the nucleus to maximize their cytotoxicity. In this study, we show that monoclonal antibodies labeled with ^{125}I (^{125}I -mAbs) and targeting the cell membrane are cytotoxic through oxidative stress-mediated nontargeted effects. As this nontargeted response is comparable to that observed with ^{125}I Urd, bystander effects induced by cell membrane irradiation could compensate for the anticipated inferior efficacy of the absence of nuclear targeting, particularly when vectors do not gain access to every tumor cell. Furthermore, Auger emitter-labeled mAbs bypass the disadvantages of using labeled deoxyribonucleotides.

review, Kassis (25)]. The majority of Auger electrons have very low energies (between a few eV and 1 keV) and thus very short range in tissue ($<1\ \mu\text{m}$). They release high amounts of energy in a spherical volume of a few cubic nanometers (46, 49, 54) and behave like medium-to-high linear energy transfer (LET) radiation (4–26 keV/ μm). Hence, they produce locally dense ionizations that are very destructive when incorporated into nuclear DNA (7, 22, 26–29) or the nucleus (1, 9, 12, 14, 15). Although they have high LET features, they have been shown to contribute to cytotoxicity or DNA lesion formation indirectly *via* reactive oxygen species (ROS) (63, 64).

The radionuclides iodine 125 (^{125}I), iodine 123 (^{123}I), and indium 111 (^{111}In) are the most widely used Auger electron emitters for *in vitro* and *in vivo* studies. Clinical trials have evaluated the efficacy, toxicity, or tumor distribution of Auger electron emitters conjugated to (i) thymidine analogs that are incorporated into the DNA of cells in S phase (18, 40, 41), (ii) octreotide, a somatostatin analog targeting neuroendocrine and other cancers (16, 31, 37), and (iii) monoclonal antibodies (mAbs) with specificity for cancer cellular antigens (35, 52, 65) and human epidermal growth factor receptor (62). The latter treatment is known as radioimmunotherapy (RIT).

Conventionally, Auger electron emitters are targeted to the nucleus or DNA because it is considered that Auger electrons need to be within the nucleus to achieve maximal cell kill. Therefore, RIT using Auger electron emitters has been regarded as comparatively disadvantageous because the localization of the radionuclide, after receptor binding, is not the nucleus, but the cytoplasm (internalizing mAbs) or the cell membrane (noninternalizing mAbs).

However, we previously showed, using *in vitro* and *in vivo* models, substantial antitumor efficacy of noninternalizing monoclonal antibodies labeled with ^{125}I (^{125}I -mAbs). Furthermore, the cytotoxicity of noninternalizing mAbs was greater than that achieved by internalizing ^{125}I -mAbs (50, 53) and was not due to inefficient detection of DNA damage related to low absorbed dosage. We proposed that, instead, nontargeted effects could be involved (48). This is in agreement with the work by Xue *et al.* in 2002 showing *in vivo* that nontargeted effects are produced by LS174T cells radiolabeled with the DNA base analog 5-[(125)I]iodo-2'-deoxyuridine (^{125}I -UdR), indicating that Auger electrons can kill cells beyond their path length (66). Other reports indicate that they have also been observed during radionuclide therapy using tritiated thymidine (3H3H-dThd) (5), meta-

[^{211}At]astatobenzylguanidine (^{211}At -MABG), meta[^{123}I]iodobenzylguanidine (^{123}I -MIBG) (6), and ^{213}Bi -mAbs (10).

Radiation-induced nontargeted effects (also called by-stander effects) occur in cells that are not directly traversed by ionizing particles, but are in contact with irradiated cells. They have been mainly observed after low-dose ($<0.5\ \text{Gy}$) external beam radiotherapy (EBRT), for both low and high LET irradiation, and are associated with a lack of dose–effect relationships [for reviews, Hamada (19) and Prise and O'Sullivan (51)]. Bystander effects include cell death, DNA damage, apoptosis (39), yield of micronuclei and chromosomal aberrations (4, 43), and malignant transformation (55). The bystander response depends both on the cell type and on radiation LET and involves the release of soluble factors in the extracellular environment together with the transmission of signaling molecules through gap junctions when cells are in contact (33, 42). ROS and reactive nitrogen species (RNS), Ca^{2+} ions, ATP, and cytokines have been shown to be involved (2, 38).

In this study, we show that oxidative stress-induced nontargeted effects are involved in the cytotoxicity of ^{125}I -mAbs targeting cell surface receptors. This phenomenon involves lipid raft formation followed by subsequent activation of signaling pathways. Moreover, the potency of the cytotoxic nontargeted effect induced by targeting the nucleus with ^{125}I -UdR was comparable to that resulting from exposure to ^{125}I -mAbs against cell surface receptors, suggesting that it was independent of the localization of Auger electron emitters. Finally, our data support the existence of nontargeted cytotoxic effects, both *in vitro* and *in vivo*.

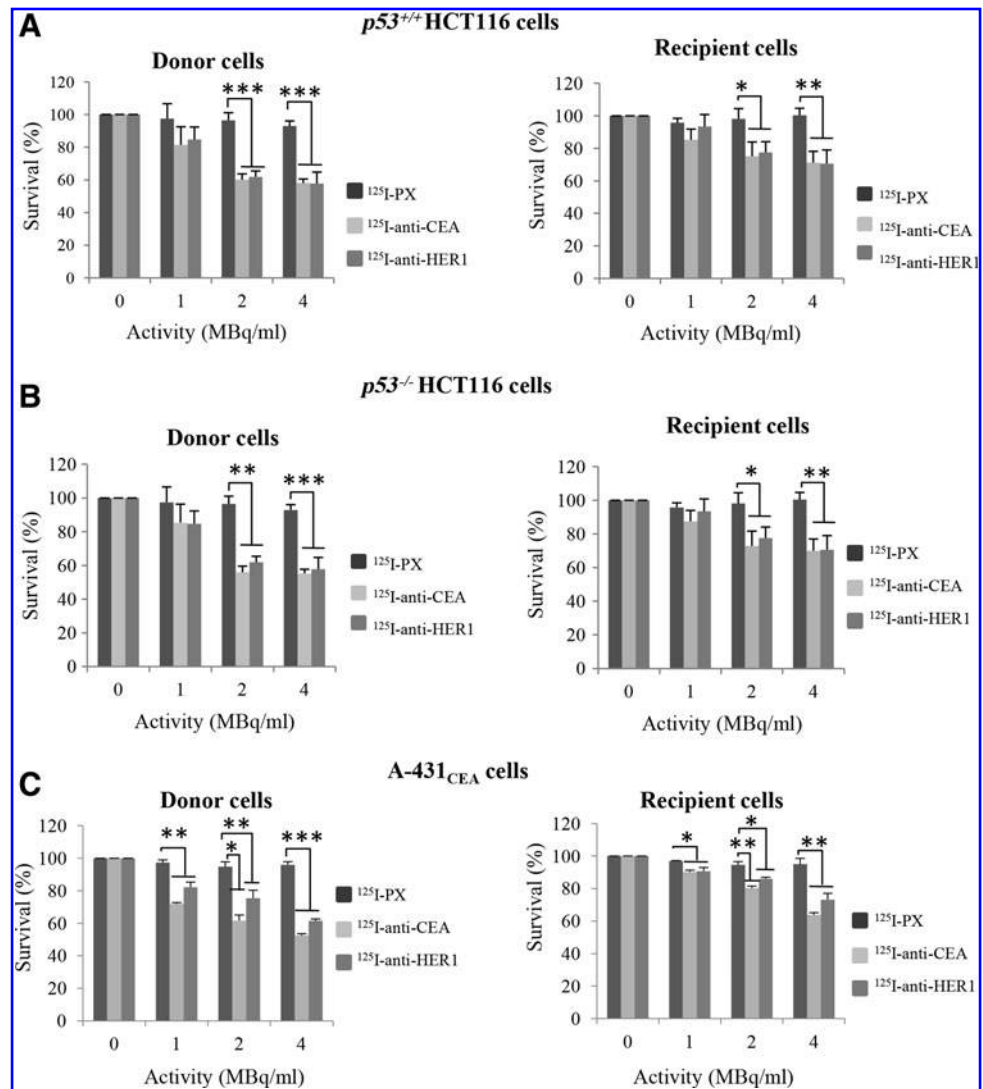
Results

^{125}I -mAbs induce nontargeted effects

Clonogenic survival of $p53^{+/+}$ HCT116 cells targeted by 4 MBq/ml of noninternalizing anti-carcinoembryonic antigen (CEA) ^{125}I -mAb (resulting in cell surface localization of ^{125}I) or internalizing anti-Human Epidermal Receptor type 1 (HER1) ^{125}I -mAb (resulting in cytoplasmic localization of ^{125}I) (donor cells) was reduced to $58\% \pm 2.5\%$ and $57.8\% \pm 7\%$, respectively. These values were significantly different ($p < 0.001$) from values measured using the nonspecific ^{125}I -PX mAb (Fig. 1A, left panel). We also investigated the role of p53 by performing the same experiments in $p53^{-/-}$ HCT116 cells and showed a similar reduction in clonogenic survival (to $54.6\% \pm 1.2\%$ and $56.5\% \pm 1.9\%$, respectively) (Fig. 1B, left panel). Again survival was statistically significantly different from survival measured after nonspecific ^{125}I -PX mAb exposure ($p < 0.001$), where no toxicity was observed (Fig. 1B, left panel).

To test whether nontargeted effects were involved in the toxicity induced by ^{125}I -mAb, nonirradiated $p53^{+/+}$ and $p53^{-/-}$ HCT116 cells (recipient cells) were incubated with medium in which donor cells had been cultured for 2 h following a 2-day exposure to 4 MBq/ml of anti-CEA or anti-HER1 ^{125}I -mAbs. Clonogenic survival of recipient cells was significantly reduced when compared to that of cells incubated with medium from cells exposed to nonspecific ^{125}I -PX mAb ($p < 0.01$). For example, in $p53^{+/+}$ HCT116 recipient cells, survival decreased to $71.2\% \pm 7.0\%$ after incubation with medium from $p53^{+/+}$ HCT116 donor cells exposed to anti-CEA ^{125}I -mAb and to $70.6\% \pm 8.4\%$ after exposure to medium from cells exposed to anti-HER1 ^{125}I -mAb (Table 1 and Fig. 1A, right panel). Similarly, in $p53^{-/-}$ HCT116 recipient cells, survival decreased to

FIG. 1. Clonogenic survival. Clonogenic survival was assessed in donor and recipient cells 12 days following either exposure to activities of ^{125}I -mAbs from 0 to 4 MBq/ml for 2 days (donor cells) or incubation in culture medium in which donor cells had been cultured for 2 h (recipient cells). Donor cells were treated with noninternalizing ^{125}I -anti-CEA, internalizing ^{125}I -anti-HER1, or nontargeting ^{125}I -PX mAbs. Clonogenic survival was measured in (A) $p53^{+/+}$ HCT116, (B) $p53^{-/-}$ HCT116, and (C) A-431_{CEA} cells. Results are the mean \pm SD of four experiments performed in triplicate. * $p < 0.05$, ** $p < 0.01$, *** $p < 0.001$ compared with ^{125}I -PX mAb-treated cells. CEA, carcinoembryonic antigen; HER1, Human Epidermal Receptor type 1; ^{125}I , iodine 125; mAbs, monoclonal antibodies; SD, standard deviation.



73.3% \pm 5.6% following incubation with medium from $p53^{-/-}$ HCT116 donor cells exposed to anti-CEA ^{125}I -mAb and to 74.5% \pm 5.1% upon switch to medium from cells exposed to anti-HER1 ^{125}I -mAb (Fig. 1B, right panel).

No cell killing was observed after incubation of recipient cells with medium from donor cells treated with the nontargeting ^{125}I -PX mAb (Fig. 1B, right panel) or with unlabeled mAbs (Supplementary Fig. S1A; Supplementary Data are available online at www.liebertpub.com/ars). This suggests that the effect was specific and required ^{125}I -mAb binding to the cell surface. Similar results were obtained in A-431_{CEA} (Fig. 1C) and SK-OV-3_{CEA} cells (Supplementary Fig. S1B) treated with the same ^{125}I -mAbs. Gamma-H2AX foci (markers of DNA double strand breaks, DSBs) were detected in both $p53^{+/+}$ HCT116 donor (exposed to anti-CEA or anti-HER1 ^{125}I -mAbs) and recipient cells, again indicating the occurrence of nontargeted effects in recipient cells (Fig. 2A, B). It must be noted that cells were proliferating and that a larger number of gamma-H2AX foci are likely to be produced during the S phase. The proportion of donor cells showing foci was assessed to be about 10% in nonirradiated cells, while it increased up to 25% in cells exposed to the nonspecific ^{125}I -PX mAb and 100% after exposure to the specific anti-HER1 and anti-CEA ^{125}I -mAbs.

Corresponding values were 15% and 100% in recipient cells (data not shown).

Nontargeted effects do not require cellular internalization of ^{125}I

Localization of the anti-CEA and anti-HER1 mAbs at the cell membrane and cytoplasm, respectively, was confirmed by cell fractionation followed by Western blotting (Fig. 2C) and by immunofluorescence (Fig. 2D) in $p53^{+/+}$ HCT116 and A-431_{CEA} cells. Coincubation of $p53^{+/+}$ HCT116 donor cells with anti-CEA or anti-HER1 ^{125}I -mAbs and sodium azide, a drug preventing antibody internalization after receptor binding, did not modify the nontargeted response in recipient cells (Fig. 2E). These results suggest that internalization of ^{125}I is not required for radiation-induced nontargeted effects.

The role of lipid rafts in ^{125}I -mAb cytotoxicity in vitro

Lipid rafts can be ceramide-enriched platforms in the cell membrane that are produced through sphingomyelin hydrolysis to ceramide and phosphorylcholine following acid sphingomyelinase (ASMase) activation by ROS (56). To investigate whether ^{125}I -mAbs affected the cell membrane

TABLE 1. ¹²⁵I SUBCELLULAR LOCALIZATION AND NONTARGETED EFFECTS

	<i>p53^{+/+}</i> HCT116 cells survival (%) at 4 MBq/ml						Contribution to HCT116 donor cell killing (%) at 4 MBq/ml	
	Total No. of decays (Bq·s/cell) at 4 MBq/ml		Donor cells		Recipient cells		Targeted cytotoxicity	Nontargeted cytotoxicity
	Nucleus	Membrane+cytoplasm	Filipin (-)	Filipin (+)	Filipin (-)	Filipin (+)		
¹²⁵ I-PX	49.8 ± 2	350.4 ± 21	92.9 ± 2.2 (7.1)	84.4 ± 2.6	98.3 ± 1.5 (1.7)	92.8 ± 2.3 (7.2)	<5.4	>1.7
¹²⁵ I-anti-CEA	45 ± 1.4	1047 ± 76	58 ± 2.5 (42)	81.0 ± 1.6 (19)	71.2 ± 7 (28.8)	94.2 ± 2.4 (5.8)	<13.2	>28.8
¹²⁵ I-anti-HER1	91 ± 1.7	14267 ± 317	57.8 ± 7 (42.2)	81.0 ± 1.6 (19)	70.6 ± 8.4 (29.4)	94.2 ± 2.4 (5.8)	<12.8	>29.4
¹²⁵ I-UdR	441 ± 27.4	14 ± 1.6	22.1 ± 1.3 (77.9)	81.0 ± 1.6 (19)	72.8 ± 2.8 (27.2)	94.2 ± 2.4 (5.8)	<50.7	>27.2

Total number of decays occurring in the nucleus and in the extranuclear subcompartments and clonogenic survival (% relative to untreated cells) of *p53^{+/+}* HCT116 donor cells exposed to 4 MBq/ml ¹²⁵I-anti-CEA, ¹²⁵I-anti-HER1, ¹²⁵I-PX mAbs, or 20 kBq/ml ¹²⁵I-UdR and of the corresponding recipient cells. Cells were incubated with ¹²⁵I-vectors for 2 days. Donor cells were exposed to ¹²⁵I-mAbs in the absence [Filipin (-)] or presence [Filipin (+)] of 2.5 μg/ml of Filipin, a lipid raft disruptor, for 6 h. Donor cells were in reality both donor and recipient cells. Therefore, the specific contribution of targeted effects to donor cell killing was calculated by subtracting the percentage of cell death in recipient cells from the percentage of cell death in donor cells. Due to the long incubation with ¹²⁵I-vectors, the contribution of nontargeted effect in donor cells might be underestimated. Italic numbers show cell death percentages compared with untreated cells.

CEA, carcinoembryonic antigen; HER1, Human Epidermal Receptor type 1; ¹²⁵I, iodine 125; ¹²⁵I-UdR, 5-[(125)I]iodo-2'-deoxyuridine; mAbs, monoclonal antibodies.

organization, the formation of lipid raft domains, as detected by cholera toxin, was monitored in donor *p53^{+/+}* HCT116 cells exposed to 4 MBq/ml of anti-CEA or anti-HER1 ¹²⁵I-mAbs for 48 h. In these cells, lipid raft formation was increased compared with nonirradiated cells (NT) or with cells incubated with the irrelevant ¹²⁵I-PX mAb (Fig. 3A). Flow cytometric analysis showed that the membrane concentration of ceramide (indicative of lipid raft formation) in cells exposed to anti-CEA or anti-HER1 ¹²⁵I-mAbs was increased compared with nonirradiated cells (NT) and cells treated with unlabeled mAbs (Fig. 3B). Codetection of ceramide and Annexin (apoptosis marker) by immunofluorescence was observed in some of the *p53^{+/+}* HCT116 cells (Fig. 3C). However, we previously showed that apoptosis was not involved in the cytotoxic effects of ¹²⁵I-anti-CEA mAb (46).

The formation of ceramide was corroborated also by the significantly higher ASMase activity measured in whole cell lysates of *p53^{+/+}* HCT116 treated with anti-CEA or anti-HER1 ¹²⁵I-mAbs (three times higher compared to unlabeled mAbs, *p* < 0.001) (Fig. 3D). We also found that the level of sphingosine-1-phosphate (S1P) resulting from hydrolysis of ceramide was strongly increased in cells exposed to anti-CEA or anti-HER1 ¹²⁵I-mAbs (Fig. 3E), while no such increase was observed in control cells.

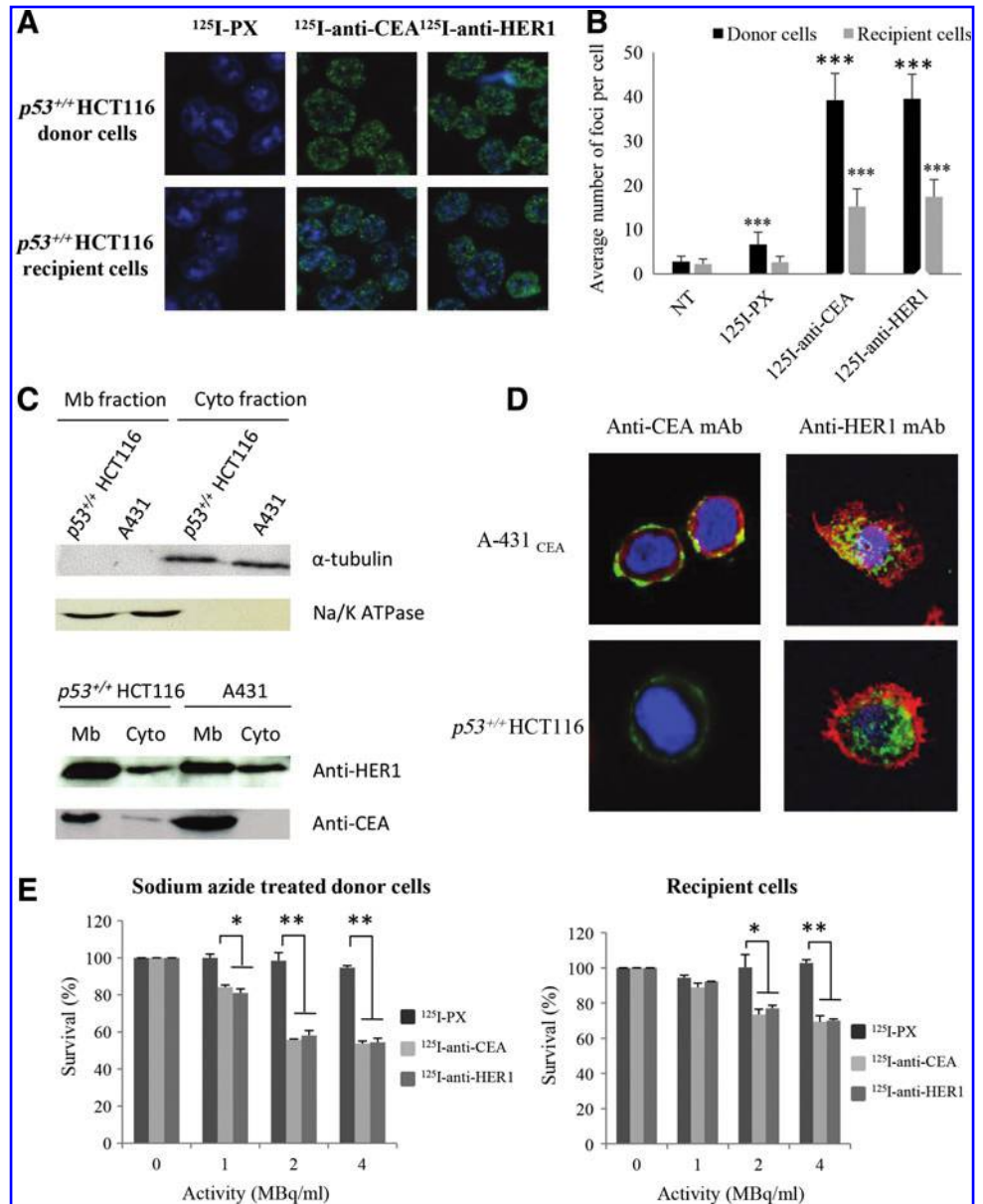
The involvement of lipid raft formation in ¹²⁵I-mAb cytotoxicity was confirmed by the finding that lipid raft formation was reduced in *p53^{+/+}* HCT116 donor cells coincubated with anti-CEA or anti-HER1 ¹²⁵I-mAbs and filipin (a lipid raft disruptive agent) compared with cells exposed only to ¹²⁵I-mAbs (Fig. 4A). Moreover, coincubation of donor cells with filipin significantly reduced the formation of phosphorylated histone H2AX (γ-H2AX) foci in both donor and recipient cells (Fig. 4B). Finally, ¹²⁵I-mAb cytotoxicity in both donor (Fig. 4C) and recipient cells (Fig. 4D) was significantly reduced when donor cells were incubated in the presence of filipin. Indeed, clonogenic survival increased from 58% ± 2.5% to 84.4% ± 2.6% and from 57.8% ± 7% to 81.0% ± 1.6% in donor cells coincubated with 4 MBq/ml anti-CEA or anti-HER1 ¹²⁵I-mAbs and filipin, respectively (Table 1). In recipient cells, survival increased from 71.2% ± 7% to 92.8% ± 2.3% and from 70.6% ± 8.4% to 94.2% ± 2.4%, respectively. Similar protection was afforded by methyl-β-cyclodextrin (MBCD), another lipid raft disruptor (Supplementary Fig. S2). These findings indicate that lipid raft formation is involved in both targeted and nontargeted cytotoxicity of ¹²⁵I-mAbs.

Phosphorylated proteins associated with ¹²⁵I-RIT

To identify the signaling pathways activated in cells exposed to anti-CEA or anti-HER1 ¹²⁵I-mAbs, the phosphorylation profiles of 46 kinases were assessed by array-based proteomics (Fig. 5 and Supplementary Fig. S3). Only extracellular signal-related kinase ½ (ERK1/2) and C-AMP Response Element-binding protein (CREB) were strongly activated after treatment with unlabeled anti-CEA mAb (Fig. 5A). Conversely, upon incubation with the unlabeled anti-HER1 mAb, several proteins were induced, including ERK1/2, CREB, p53, and AKT (Fig. 5B).

Thus, only the anti-CEA ¹²⁵I-mAb was used to investigate the effect of targeting ¹²⁵I to the cell surface. When cells were exposed to anti-CEA ¹²⁵I-mAb (Fig. 5A), the ERK1/2, AKT, p38, and c-Jun N-terminal kinase (JNK) signaling pathways

FIG. 2. Gamma-H2AX foci detection and optional role of ^{125}I -mAb internalization for nontargeted cytotoxicity. (A) Detection of gamma-H2AX foci in $p53^{+/+}$ HCT116 donor cells (top panels) and recipient cells (bottom panels) by immunofluorescence assay. (B) The number of foci per cell was counted in 100 cells. Antibody localization was assessed in $p53^{+/+}$ HCT116 and A-431_{CEA} cells by (C) subcellular fractionation and (D) immunofluorescence. F-actin was stained with conjugated phalloidin (Red) to visualize cytoplasm, nuclei with Hoechst (Blue), and mAbs with Alexa-488-conjugated anti-mouse secondary mAbs. (E) Clonogenic survival was assessed in $p53^{+/+}$ HCT116 donor cells coincubated with 0.02% sodium azide (a drug blocking antigen internalization) and a range of activities of ^{125}I -mAbs (non-internalizing anti-CEA, internalizing anti-HER1, or nontargeting PX mAbs). Clonogenic survival of recipient cells was assessed after incubation with conditioned medium from donor cells exposed to ^{125}I -mAbs in the presence of sodium azide. Results are the mean \pm SD of three experiments performed in triplicate. * $p < 0.05$, ** $p < 0.01$, and *** $p < 0.001$ compared to NT cells (B) or to the ^{125}I -PX mAb-treated cells (E). Mb, membrane; Cyto, cytoplasm. To see this illustration in color, the reader is referred to the web version of this article at www.liebertpub.com/ars



were induced. Activated downstream AKT proteins included p70S6 kinase (p70S6K), glycogen synthase kinase 3 (GSK3), and endothelial nitric oxide synthase (e-NOS) (61). Signal transducer and activator of transcription (STAT) 1 and 4, 90 kDa ribosomal S6 kinase (RSK), mitogen- and stress-activated protein kinase (MSK), and CREB proteins, which are downstream targets of ERK1/2 signaling, were also activated, as well as c-JUN, which is downstream of p38 and JNK (for review (61)). Phosphorylated proteins involved in Ca^{2+} fluxes, such as phospholipase C- γ (PLC- γ), proline-rich tyrosine kinase 2 (PYK-2), and paxillin, were strongly activated by exposure to anti-CEA ^{125}I -mAb. Phosphorylation of AKT, p38, JNK, CREB, GSK3, STAT 1 and 4, e-NOS, MSK, PLC- γ , PYK-2, and paxillin was abolished, whereas phosphorylation of ERK1/2, c-JUN, p53, RSK, SAT 2, and p70S6K was diminished in cells coincubated with filipin (Fig. 5), confirming that these proteins are downstream ef-

factors of lipid raft formation and, thus, are likely to be involved in ^{125}I -mAb nontargeted effects. Moreover, the use of different pharmacological inhibitors of MEK (U0126) and subsequently of downstream ERK1/2 signaling pathway, PI3K (ZSTK474) and subsequently of downstream AKT signaling pathway, p38 (SB203580), and JNK (SP600125) indicated that, among the identified proteins activated, p38 and JNK were mainly involved in the response of cells to ^{125}I -mAb exposure (Fig. 6). No effect of EGTA on clonogenic survival was observed (Supplementary Fig. S1C).

ROS are involved in Auger electron-induced nontargeted response

The involvement of ROS in the mediation of the bystander response was examined by culturing recipient cells in medium from $p53^{+/+}$ HCT116 donor cells that had been treated

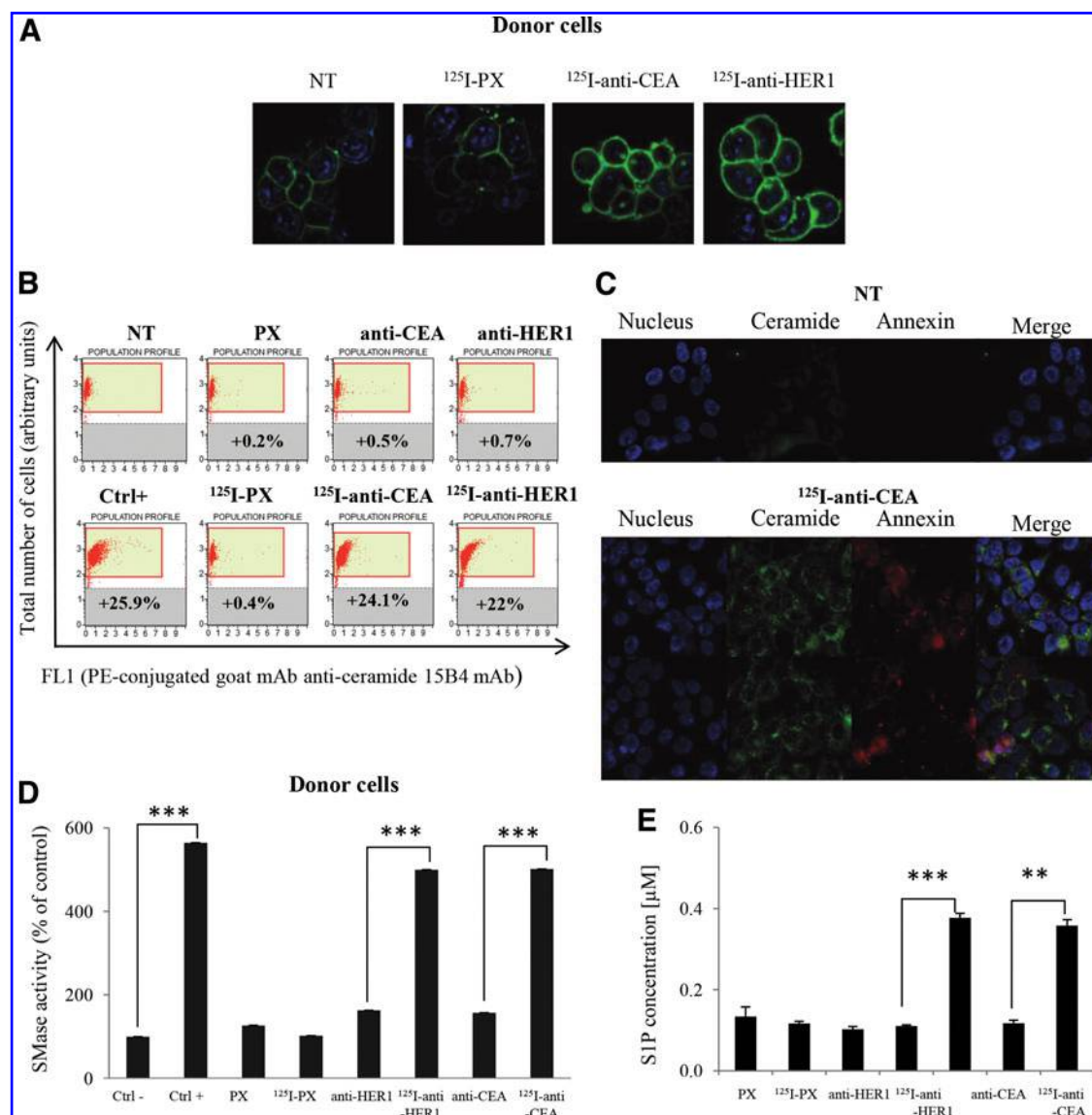


FIG. 3. Lipid rafts are formed upon exposure to ^{125}I -mAbs via ASMase-induced ceramide formation. (A) Lipid rafts were detected by immunofluorescence analysis using Alexa-488-conjugated cholera toxin (a marker of lipid raft) in untreated (NT) and treated $p53^{+/+}$ HCT116 cells (nontargeting ^{125}I -anti-CEA, internalizing ^{125}I -anti-HER1, nontargeting ^{125}I -PX mAbs). (B) Ceramide was measured in $p53^{+/+}$ HCT116 cells by flow cytometry analysis after treatment with unlabeled mAbs (top panels), or with ^{125}I -mAbs (bottom panels). Ctrl+, positive control (100 μl of 0.4 U/ml *Bacillus cereus* SMase and 10 μl sphingomyelin). (C) Colocalization of ceramide and Annexin V in apoptotic cells was determined by immunofluorescence, in untreated (NT) and ^{125}I -anti-CEA-treated $p53^{+/+}$ HCT116 cells. (D) ASMase activity was determined in whole $p53^{+/+}$ HCT116 cell lysates using the Amplex Red Sphingomyelinase Fluorimetry Kit after incubation with unlabeled or ^{125}I -mAbs. Ctrl+, positive control (100 μl of 0.4 U/ml *B. cereus* SMase and 10 μl sphingomyelin); Ctrl- (Amplex Red working solution without sphingomyelin). (E) S1P concentration was determined in whole $p53^{+/+}$ HCT116 cells lysates using the Sphingosine-1-Phosphate Assay Kit after incubation with unlabeled or ^{125}I -mAbs or in nontreated cells (NT). Results are the mean \pm SD of four experiments performed in triplicate. $**p < 0.01$ and $***p < 0.001$ compared to cells treated with unlabeled mAbs. ASMase, acid sphingomyelinase; S1P, sphingosine-1-phosphate. To see this illustration in color, the reader is referred to the web version of this article at www.liebertpub.com/ars

with ^{125}I -mAbs in the presence or absence of the free radical scavengers dimethyl sulfoxide (DMSO) or N-acetylcysteine (NAC) (Fig. 7). We previously checked (using immunofluorescence detection of mAbs in the presence of cells grown on coverslips) that NAC did not prevent anti-HER1 or anti-CEA mAbs from binding to their receptors.

Survival of both donor and recipient cells was significantly increased compared with controls treated with ^{125}I -mAbs in the absence of free radical scavengers ($p < 0.001$ and $p < 0.01$,

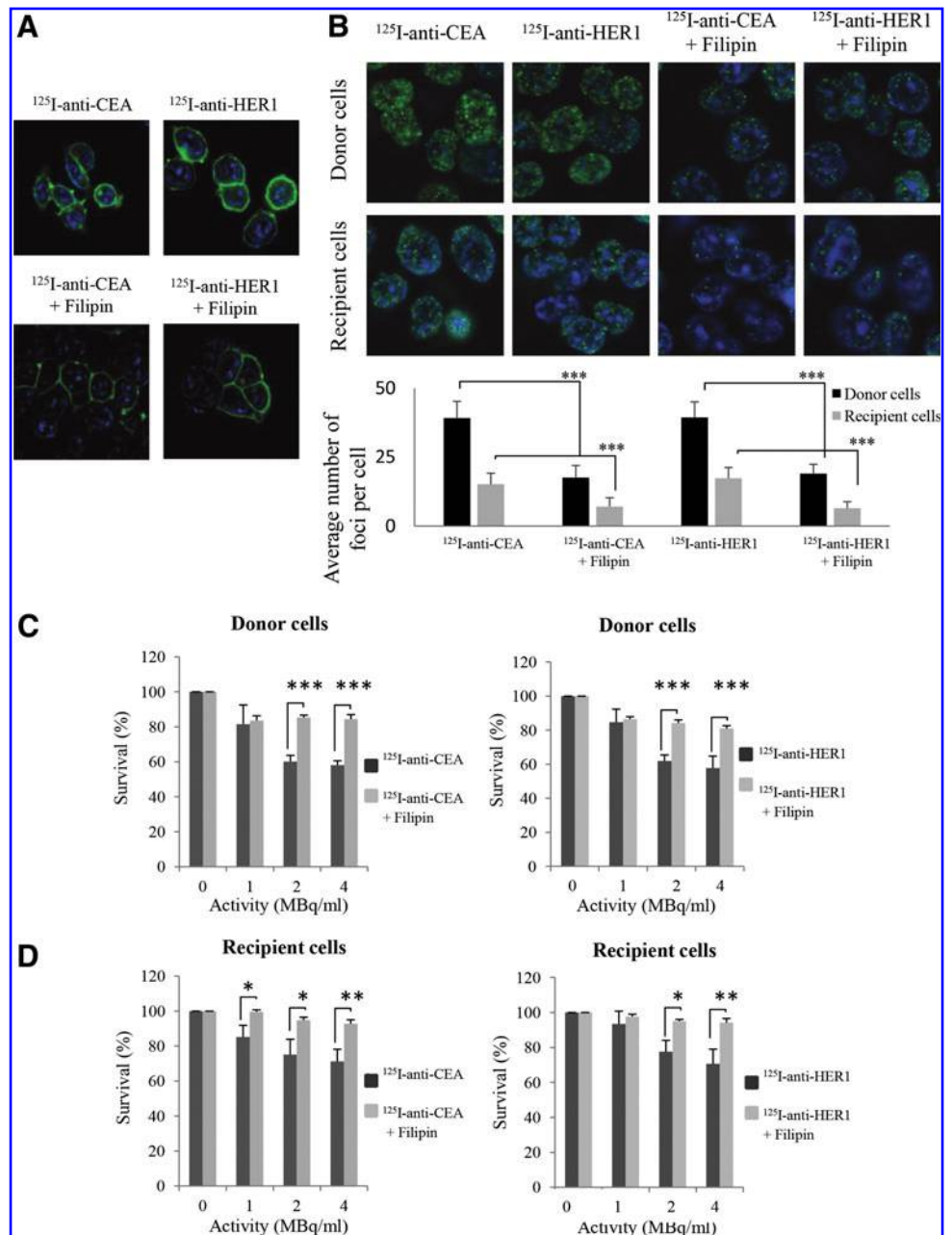
respectively). This suggests that oxidative stress is involved in both targeted and nontargeted cytotoxic effects of ^{125}I -mAbs.

Nontargeted effects of ^{125}I directed to the cell membrane or the nucleus are equipotent

To compare the effect of targeting ^{125}I to the cell membrane or the nucleus, $p53^{+/+}$ HCT116 donor cells were incubated with ^{125}I -UdR (nuclear localization of ^{125}I) or with anti-CEA or anti-HER1

FIG. 4. Role of lipid rafts in the nontargeted response.

(A) Disruption of lipid rafts was confirmed by immunofluorescence analysis using Alexa-488 (Green)-conjugated cholera toxin (a marker of lipid rafts) in $p53^{+/+}$ HCT116 cells coincubated with ^{125}I -mAbs (non-internalizing anti-CEA or internalizing anti-HER1) and filipin. Nuclei were stained with Hoechst (Blue). (B) Images of gamma-H2AX foci (immunofluorescent detection of Alexa-488 [Green] conjugated anti mouse-anti gamma-H2AX antibody) in $p53^{+/+}$ HCT116 donor cells incubated 2 days with ^{125}I -mAbs in the presence or absence of filipin (top panels) and in the corresponding recipient cells (bottom panels). The number of foci per cell was counted in 100 cells. Clonogenic survival was assessed in $p53^{+/+}$ HCT116 donor cells coincubated for 2 days with and without ^{125}I -mAbs and filipin (C), and in the corresponding recipient cells (D). Results are the mean \pm SD of four experiments performed in triplicate. * $p < 0.05$, ** $p < 0.01$, *** $p < 0.001$ compared to cells treated with ^{125}I -mAbs. To see this illustration in color, the reader is referred to the web version of this article at www.liebertpub.com/ars



^{125}I -mAbs. Subsequently, clonogenic survival was assessed in both donor and recipient cells. Results are summarized in Table 1. The uptake of ^{125}I -UdR and ^{125}I -mAbs was measured for every test activity for 6 days, and the total number of decays occurring in cells was calculated as described previously (46). The results of the clonogenic survival assay showed that, in donor cells, ^{125}I -UdR (nuclear localization) was more cytotoxic than anti-CEA (cell surface localization) or anti-HER1 (cytoplasmic localization) ^{125}I -mAbs. Conversely, in recipient cells, cell survival was similar and independent of ^{125}I localization, indicating that ^{125}I at the cell membrane is as efficient as nuclear ^{125}I in killing bystander cells.

The role of lipid rafts in ^{125}I -mAb cytotoxicity in vivo

Mice bearing intraperitoneal tumor xenografts were treated with NaCl, anti-CEA mAb (100 μg /injection at day 8 and 11), ^{125}I -anti-CEA mAb (37 MBq/injection at day 8 and 11), or

MBCD (300 mg/kg; daily, from day 6 to 15), or with both ^{125}I -anti-CEA mAb and MBCD. At day 30, tumor mass was significantly reduced in the group treated with ^{125}I -anti-CEA mAb (RIT) compared with the NaCl group ($p = 0.0227$). No difference was observed between the groups treated with MBCD, NaCl ($p = 0.9349$), or anti-CEA mAb ($p = 0.9563$). The latter result is in agreement with a previously published study indicating that anti-CEA mAbs have no effect on mouse tumor growth (53). Treatment with MBCD removed the statistical significance of RIT-induced tumor growth delay such that no difference was observed between NaCl and RIT+MBCD groups ($p = 0.2481$) (Fig. 8A).

Oxidative DNA damage occurs beyond the range of Auger electrons in vivo

Digital autoradiographic analysis performed on sections of tumors collected in mice injected with ^{125}I -anti-CEA mAb

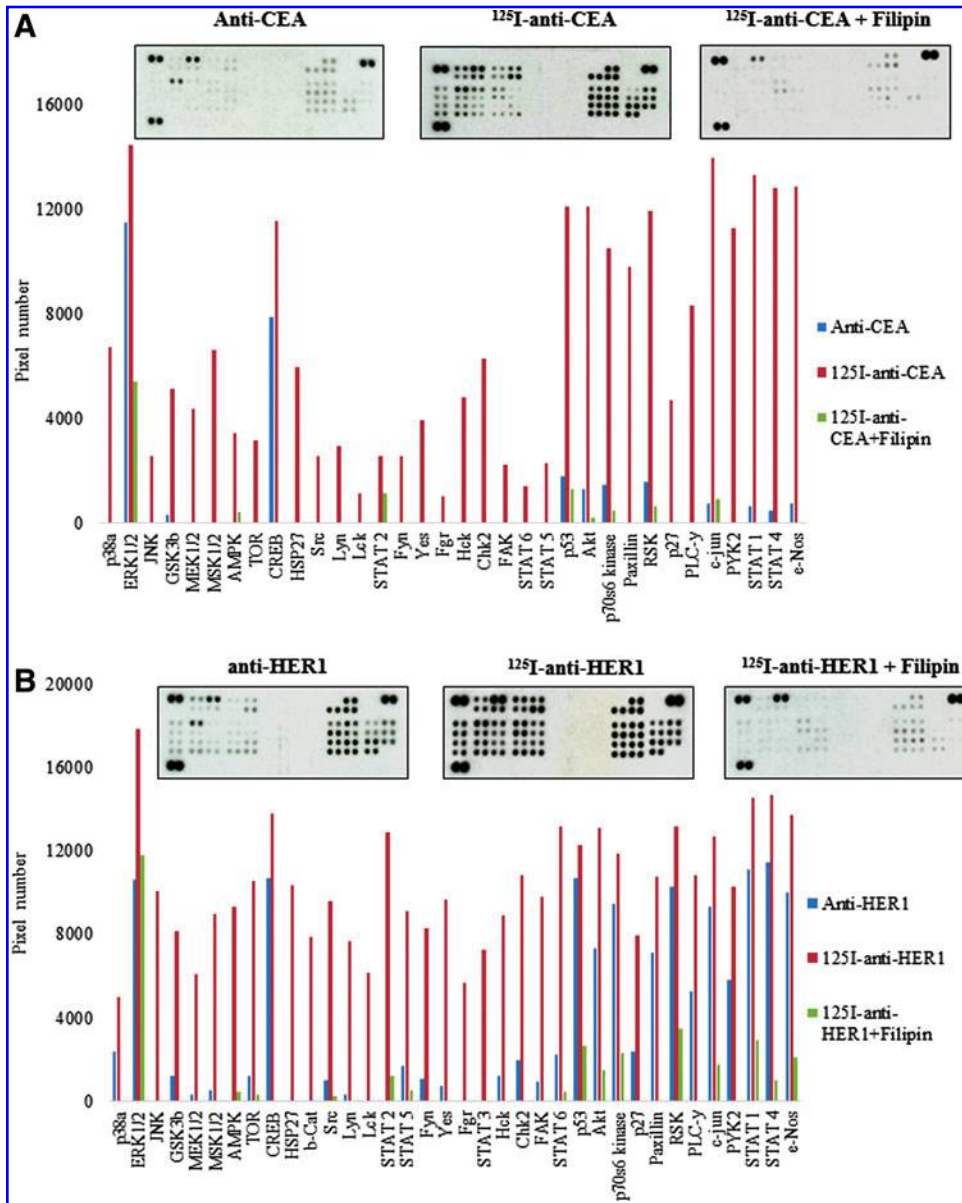


FIG. 5. Signaling pathways activated in ^{125}I -mAb-treated $p53^{+/+}$ HCT116 cells and role of oxidative stress in the nontargeted response. (A) Signaling pathways activated after incubation of $p53^{+/+}$ HCT116 donor cells with unlabeled anti-CEA, anti-CEA ^{125}I -mAbs, or anti-CEA ^{125}I -mAbs and filipin. (B) Signaling pathways activated after incubation of $p53^{+/+}$ HCT116 donor cells with unlabeled anti-HER1, anti-HER1 ^{125}I -mAbs, or anti-HER1 ^{125}I -mAbs and filipin. The Human Phospho-Kinase array (Proteome Profiler Array; R&D Systems, Minneapolis, MN) was used to detect the phosphorylation level of 46 kinases. For each kinase, the Image J software was used to determine pixel number. To see this illustration in color, the reader is referred to the web version of this article at www.liebertpub.com/ars

showed that radioactivity (and thus the absorbed dose) was mainly localized at the tumor periphery in A-431_{CEA} tumor cell xenografts (Fig. 9A, inset in the bottom left corner). Conversely, DNA DSBs occurred homogeneously throughout the tumor, as indicated by immunofluorescence detection of p53-binding protein 1 (53BP1), a DNA damage sensor that is recruited to damaged chromatin (Fig. 9A). The average number of foci per cell was 4.4 at the center and 4.3 at the periphery of the tumor. The corresponding regional activities were 2.3 and 34.7 cpm per mm². Our observation of similar levels of DNA DSBs at the center of the tumor, independent of the absorbed dose and beyond the range of Auger electrons, supports the involvement of nontargeted effects also *in vivo*. 53BP1 expression was also investigated in A-431_{CEA} tumor cell xenograft sections from mice injected with the irrelevant ^{125}I -PX mAb (Fig. 9B). The numbers of foci per cell was 0.8 (tumor center) and 1.0 (tumor periphery). These values were lower than those observed following treatment with anti-CEA ^{125}I -mAb, de-

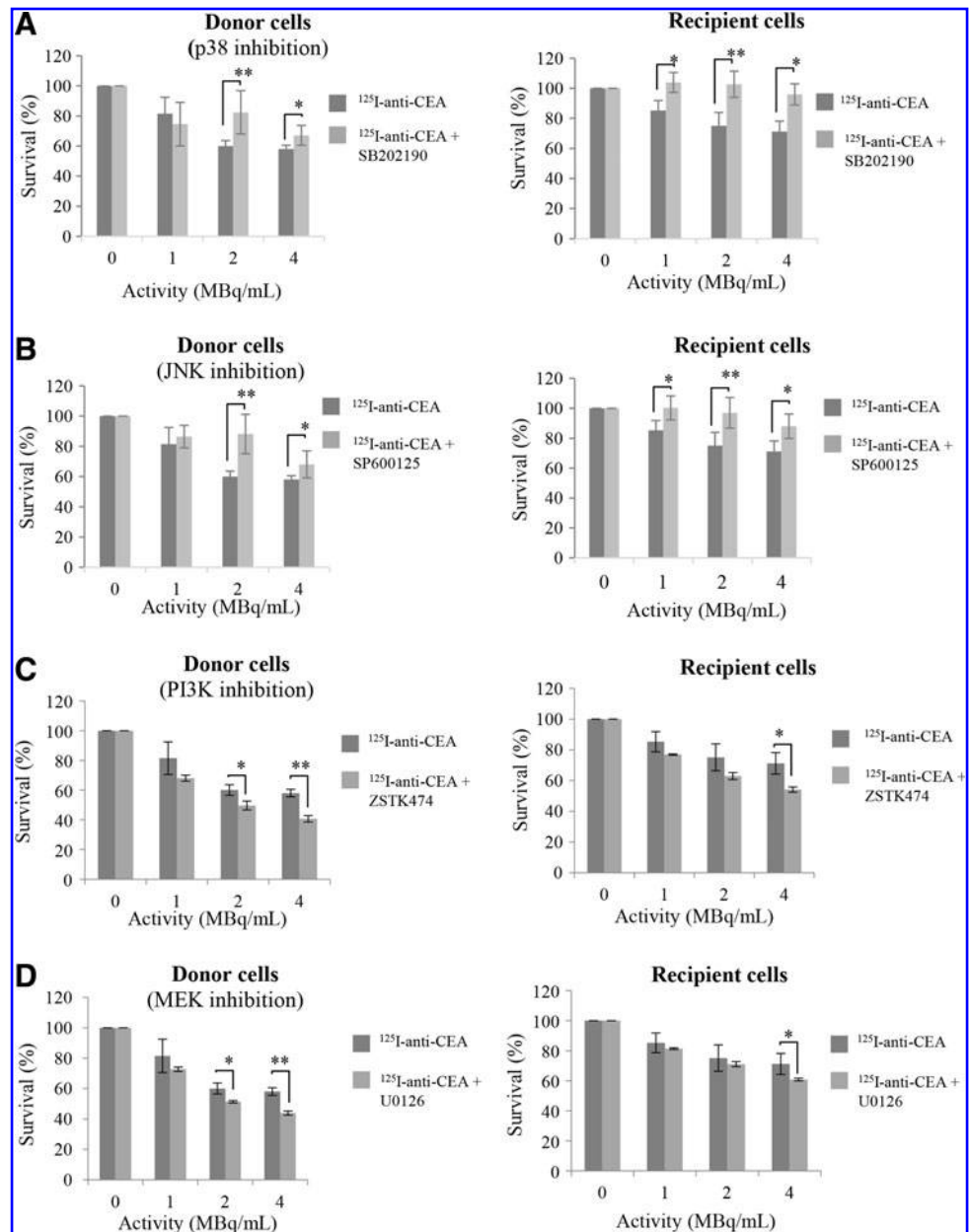
spite the higher uptake of ^{125}I -PX mAb exemplified by activity per area values of 28 and 18.2 cpm/mm² at the tumor center and periphery, respectively. A similar level of 0.7 \pm 0.1 53BP1 foci was found in tumors of NaCl or anti-CEA-treated mice (Fig. 9C).

This ruled out the possibility that the signal detected in tumors treated with anti-CEA ^{125}I -mAb was caused by non-specific induction of 53BP1 due to cross-irradiation from the radioactivity present in nonmalignant regions of the animal.

Discussion

In the present study, we show that ^{125}I translocation to the nucleus is not required for cell killing and that radiation-induced nontargeted effects contribute to ^{125}I cytotoxicity when labeled with monoclonal antibodies (^{125}I -mAbs) (Table 1). We also identify the signaling pathways involved in these nontargeted effects. In particular, we show using $p53^{-/-}$ and $p53^{+/+}$ HCT116 cells that the latter protein did not play a

FIG. 6. Pharmacological inhibitors of MAPK pathways. *p53*^{+/+}HCT116 donor cells were incubated for 48 h with ¹²⁵I-anti-CEA mAb in the presence of (A) SB203580 (p38 inhibitor), (B) SP600125 (JNK inhibitor), (C) ZSTK474 (PI3K inhibitor and indirectly of its downstream AKT pathway), or (D) U0126 (MEK1/2 inhibitor and indirectly of its downstream ERK1/2 pathway). Results are the mean \pm SD of four experiments performed in triplicate. **p* < 0.05, ***p* < 0.01, compared to cells treated with ¹²⁵I-mAbs. ERK1/2, extracellular signal-related kinase 1/2; JNK, c-Jun N-terminal kinase; MAPK, mitogen-activated protein kinase.



significant role in anti-CEA ¹²⁵I-mAb cytotoxicity since no difference was observed between the two cell lines (Fig. 1A, B and Supplementary Fig. S4). We chose the nuclear p53 protein as it is one of the main proteins involved in signaling pathways activated by nuclear damage.

The potency of nontargeted cell kill, assessed using a medium transfer protocol, was independent of ¹²⁵I localization (nucleus, cytoplasm, or cell surface) and of the magnitude of targeted cytotoxicity in donor cells (Table 1). In our *in vitro* experimental RIT model, donor cells were incubated with ¹²⁵I-mAbs and were killed both by targeted and nontargeted effects. Therefore, it is possible to determine the relative contribution of targeted and nontargeted cytotoxicity to donor cells by comparing the survival values of donor and recipient cells reported in Table 1. As death of recipient cells (incubated in culture medium in which donor cells had been cultured for 2 h) ranged between 28.8% and 29.4% (Fig. 1B),

it may be assumed that a similar (or even higher) magnitude of nontargeted effects also occurred in donor cells that were directly exposed to ¹²⁵I-mAbs for 48 h. Accordingly, cell death by targeted effects in donor cells would be equal to or less than 13.2% (42.0% minus 28.8%) and 12.8% (42.2% minus 29.4%) for ¹²⁵I localized at the cell surface or cytoplasm, respectively, and equal to or less than 50.7% (77.9% minus 27.2%) for ¹²⁵I within the nucleus (Table 1). These data confirm the greater cytotoxicity of ¹²⁵I when incorporated into DNA (22, 17, 64) in cells that are directly targeted.

Our results indicate that the cell membrane plays a major role not only in the targeted cytotoxic effects of ¹²⁵I-mAbs but also in nontargeted cytotoxic effects (Fig. 1). According to the fluid mosaic model (57), the membrane contains sphingolipids (predominantly sphingomyelin), cholesterol, and glycopospholipids. Sphingolipids associate with each other and with cholesterol to form sphingolipid- and

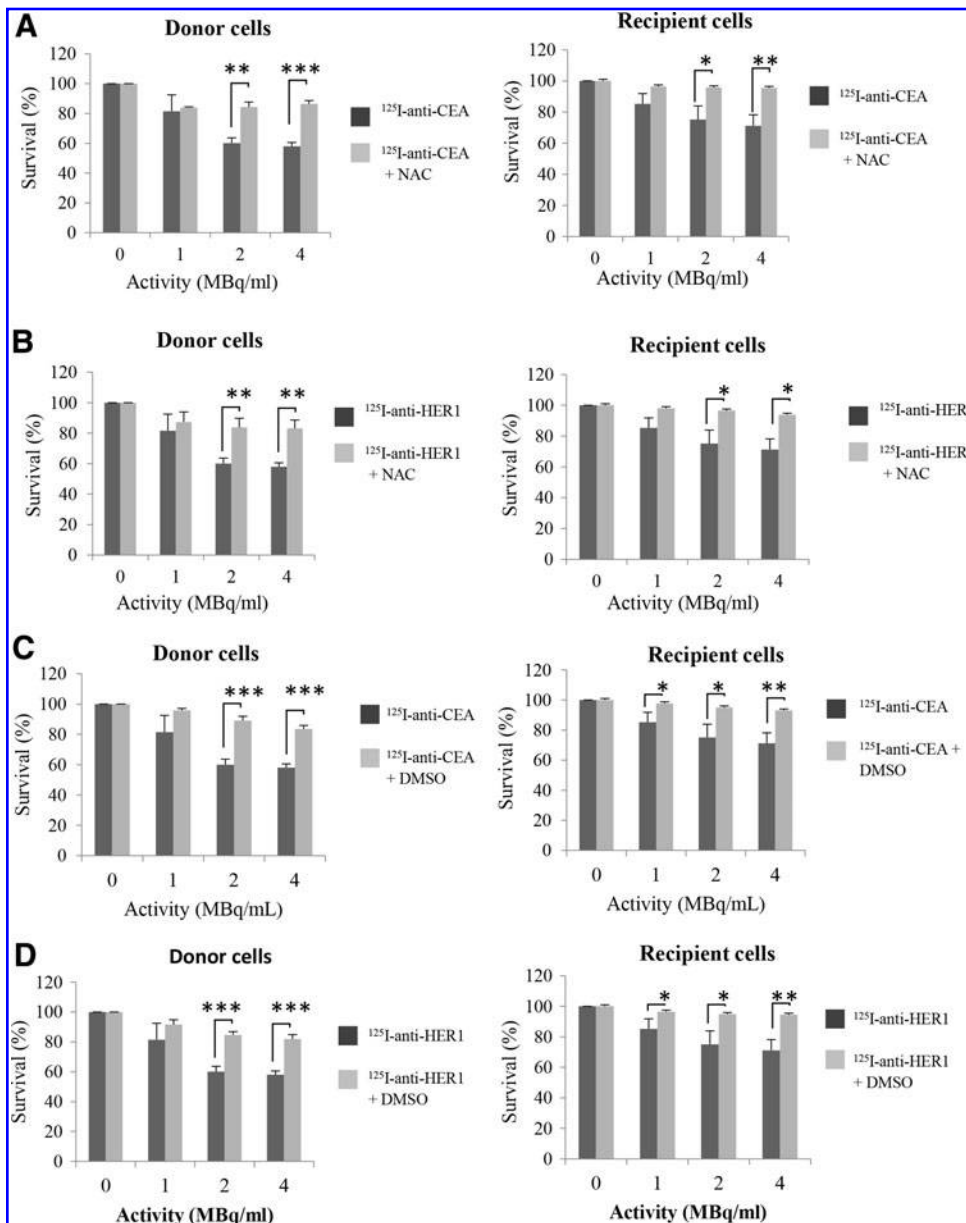


FIG. 7. Oxidative stress is involved in direct and non-targeted cytotoxicity: Effect of NAC on RIT-induced effects. $p53^{+/+}$ HCT116 donor cells were coincubated for 2 days with $50\ \mu\text{M}$ NAC or 0.5% DMSO and ^{125}I -anti-CEA (A, C, respectively) or ^{125}I -anti-HER1 (B, D, respectively) mAbs. Clonogenic survival of the donor cells and of the corresponding recipient cells was measured. Results are the mean \pm SD of four experiments performed in triplicate. * $p < 0.05$, ** $p < 0.01$, *** $p < 0.001$ compared to cells treated with ^{125}I -mAbs. DMSO, dimethyl sulfoxide; NAC, N-acetyl-L-cysteine; RIT, radioimmunotherapy.

cholesterol-enriched domains called lipid rafts that are stabilized in some cells by caveolin (32). It has been shown that ASMase activated by hydroxyl radicals (56) translocates from the cytoplasm to the outer layer of the cell membrane, where it hydrolyzes sphingomyelin into hydrophobic ceramide and hydrophilic phosphorylcholine (59, 68). Ceramide production is accompanied by the coalescence of lipid raft microdomains into ceramide-enriched large platforms that can participate in the spatial reorganization of membrane receptors and in the activation of multiple signaling pathways. Several mechanisms leading to protein activation through membrane reorganization have been identified in response to EBRT (8, 13, 47).

Our results confirm that similar mechanisms might be involved in ^{125}I -mAb efficacy after binding to the cell surface because we show that the localized energy deposition associated with ^{125}I decays was accompanied by ASMase activation (Fig. 3D), formation of ceramide-enriched large

platforms (Fig. 3A), and subsequent activation of signaling pathways (Fig. 5). ROS scavenging or disruption of lipid rafts, using MBCD or filipin, reduced not only the targeted cytotoxic effect of ^{125}I -mAbs but also the nontargeted cytotoxic effect (Figs. 4 and 7). The use of filipin, a cholesterol-depleting agent, reduced the cytotoxic effect of 4 MBq/ml anti-CEA or anti-HER1 ^{125}I -mAbs by about half in donor cells and by 75%–80% in recipient cells (Table 1), showing the involvement of lipid rafts in the cytotoxic effects of ^{125}I -mAbs. These results are supported by *in vivo* data showing that MBCD treatment removes the statistical significance of the therapeutic efficacy of ^{125}I -anti-CEA mAb (Fig. 8).

A schematic representation of the mechanisms that might be involved in ^{125}I -mAbs targeted cytotoxicity is proposed in Figure 10. Formation of ceramide-enriched large platforms is induced following ASMase activation mediated by ROS (56) originating from water radiolysis (presumably in a dose-dependent manner) (Fig. 3D). ROS could also be generated

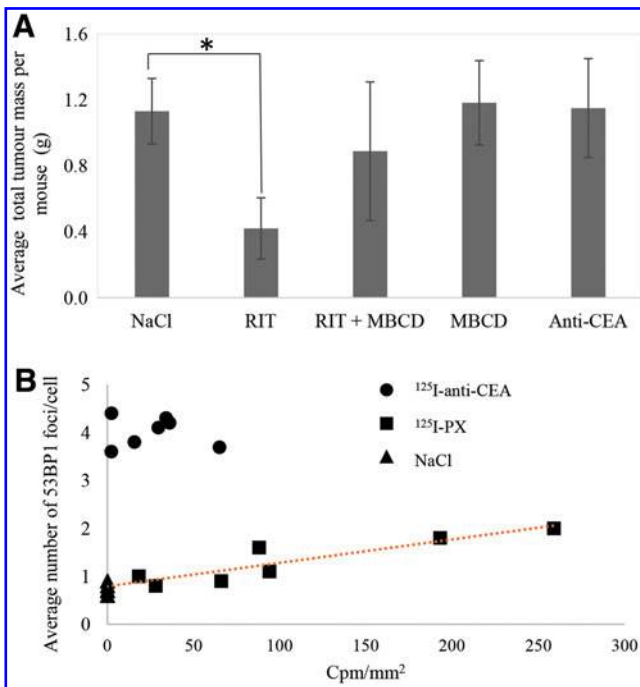


FIG. 8. *In vivo* therapeutic efficacy of ^{125}I -mAbs with or without MBCD. **(A)** Mice bearing intraperitoneal A-431_{CEA} tumor xenografts were treated with NaCl, unlabeled anti-CEA mAb (100 μg /injection at day 8 and 11), or with ^{125}I -anti-CEA mAb (RIT) at day 8 and 11 postgraft, daily with MBCD from day 6 to 15 postgraft (MBCD), or with ^{125}I -anti-CEA mAb (day 8 and 11 postgraft) and MBCD (daily from day 6 to 15 postgraft) (RIT+MBCD) ($n = 8$ mice/group). Tumors were collected at days 30 postgraft, and the total tumor mass was determined. **(B)** The level of 53BP1 was determined by immunofluorescence in cryocut slices of tumors of mice treated with 37 MBq of ^{125}I -anti-CEA mAbs, ^{125}I -PX mAbs (RIT), or with NaCl. The level was determined in 100 cells of a selected area and was correlated with the level of radioactivity (cpm/mm²) of the same area. Between 6 and 7 areas of tumors in different mice were selected. In **A**, results are the mean \pm SD of eight values. * $p < 0.05$ compared to mice treated with NaCl. 53BP1, p53-binding protein 1; MBCD, methyl- β -cyclodextrin.

following lipid raft-mediated activation of NAD(P)H oxidase (36, 67). ROS contribute to “chronic” oxidative stress and the subsequent DNA damage, including the formation of micronuclei in nontargeted cells (3, 44). This is in agreement with our previous finding that the abundance of micronuclei in cells exposed to ^{125}I -mAbs was not correlated with the mean absorbed dose to the nucleus (48, 50). The involvement of oxidative stress in EBRT-induced nontargeted effects has been extensively reviewed by Havaki *et al.* (20). Irradiated cells produce ROS and RNS through radiolysis and cytokines. ROS and RNS are then directly transmitted to bystander cells through gap junctions or through release in the extracellular medium (20). In bystander cells, different signaling pathways participate in the upregulation of genes encoding cytokines, cyclooxygenase-2 (COX2), and inducible nitric oxide synthase (iNOS) that generate intracellular ROS and RNS (20). However, the involvement of such mechanisms following low dose rate and protracted exposure (as in RIT) needs to be confirmed. The present study focused on the

mechanisms involved in irradiated donor cells, and we assume that the main source of oxidative stress was associated with radiation and hydroxyl radical formation. Elucidation of the precise mechanisms involved in recipient cells would require further work.

It is noteworthy that ^{125}I decays must occur at the surface of targeted cells to initiate the nontargeted response. Indeed, our data show that low LET radiation (including electrons and soft X-rays) emitted by the irrelevant PX ^{125}I -mAb, which does not interact with cells, did not produce a significant nontargeted response. This suggests that nontargeted effects are induced mainly by high LET Auger electrons (of very low range) generated at the cell surface when ^{125}I -mAbs bind to CEA or HER1 receptors.

The relative contribution of the various signaling pathways activated by cell membrane reorganization following lipid raft formation is complex and remains to be elucidated. We show that the mitogen-activated protein kinases (MAPKs), ERK1/2, P38, JNK, and AKT, and their downstream proteins, are activated during exposure to ^{125}I -mAbs. The role of these kinases in our model is still unclear because AKT and ERK1/2 promote cell survival, while ceramide, p38, JNK, and its downstream target c-JUN participate in cell death. However, the use of p38 or (to a lesser extent) of JNK inhibitors was accompanied by a stronger effect on clonogenic survival (increase) than the use of PI3K or MEK inhibitors, suggesting the cell death mechanisms predominate (Fig. 6). We also found that SIP, the hydrolysis product of sphingosine that is generated from ceramide by ceramidase (Figs. 3E and 10), was up-regulated following exposure to anti-CEA ^{125}I -mAb. Contrary to ceramide, SIP inhibits apoptosis and stimulates cell proliferation through activation of the AKT and e-NOS pathways [for review, Oskouian and Saba (45)]. Paxillin also was activated by incubation with anti-CEA ^{125}I -mAb (Fig. 5). Paxillin can be phosphorylated by focal adhesion kinase (FAK) or PYK-2, and phosphorylated paxillin serves as a scaffold protein to facilitate the functional integration of focal adhesion proteins. Paxillin is phosphorylated during EBRT as a downstream protein target (together with AKT and ERK1/2) of FAK (21).

Moreover, our data suggest a possible role of ion channels located in lipid rafts, such as Ca^{2+} channels. The role of Ca^{2+} in EBRT-associated nontargeted effects has clearly been demonstrated (38). The influx of extracellular Ca^{2+} can be regulated by ceramide (11), but also by PLC- γ that is activated upon exposure to anti-CEA ^{125}I -mAb (Fig. 5A). During EBRT, PLC- γ localized at the plasma membrane produces inositol triphosphate (IP₃) that consequently induces Ca^{2+} release from the endoplasmic reticulum through IP₃ receptors (60). Such an increase in Ca^{2+} cytoplasmic concentration could also contribute to the phosphorylation of PYK-2 observed in cells exposed to anti-CEA ^{125}I -mAb (Fig. 5A) (34). PYK-2, a member of the FAK family, is involved in cell proliferation and phosphorylates paxillin. However, incubation of donor cells with EGTA, a chelator of extracellular calcium, was not accompanied by modifications in clonogenic survival. In a previous study, Lyng *et al.* have used EGTA in combination with verapamil and nifedipine to block also voltage-dependent calcium channels (38) to investigate the role of Ca^{2+} ions. Such an approach merits further investigation in our models also.

Finally, we investigated in A-431_{CEA} tumor xenografts from mice injected with anti-CEA ^{125}I -mAb whether the induction of DNA DSBs could be correlated with the

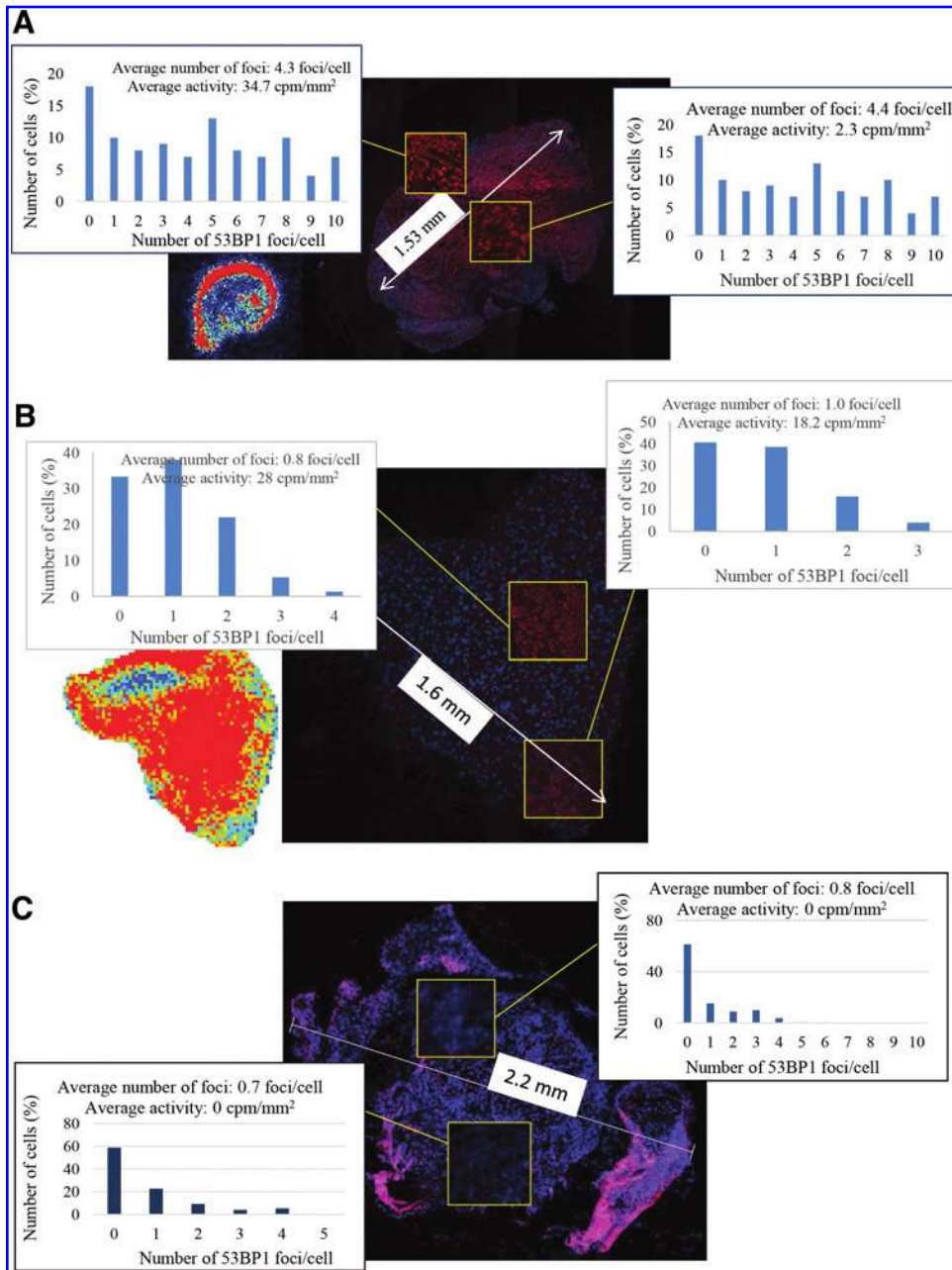


FIG. 9. Radioactivity distribution and 53BP1 induction do not overlap in A-431_{CEA} tumor cell xenografts treated with ¹²⁵I-anti-CEA mAbs. Digital autoradiography (*inset on the bottom left side of each panel*) and immunohistochemical detection of 53BP1 in tumor sections from mice xenografted intraperitoneally with A-431_{CEA} cells and treated 24 h before tissue collection with a single intraperitoneal injection of 37 MBq of (A) ¹²⁵I-anti-CEA mAb, (B) ¹²⁵I-anti-PX mAb, or (C) injected with NaCl. The distribution of 53BP1 foci was determined in 100 cells of relevant areas of tumors. Between 6 and 7 areas of tumors in different mice were selected. To see this illustration in color, the reader is referred to the web version of this article at www.liebertpub.com/ars

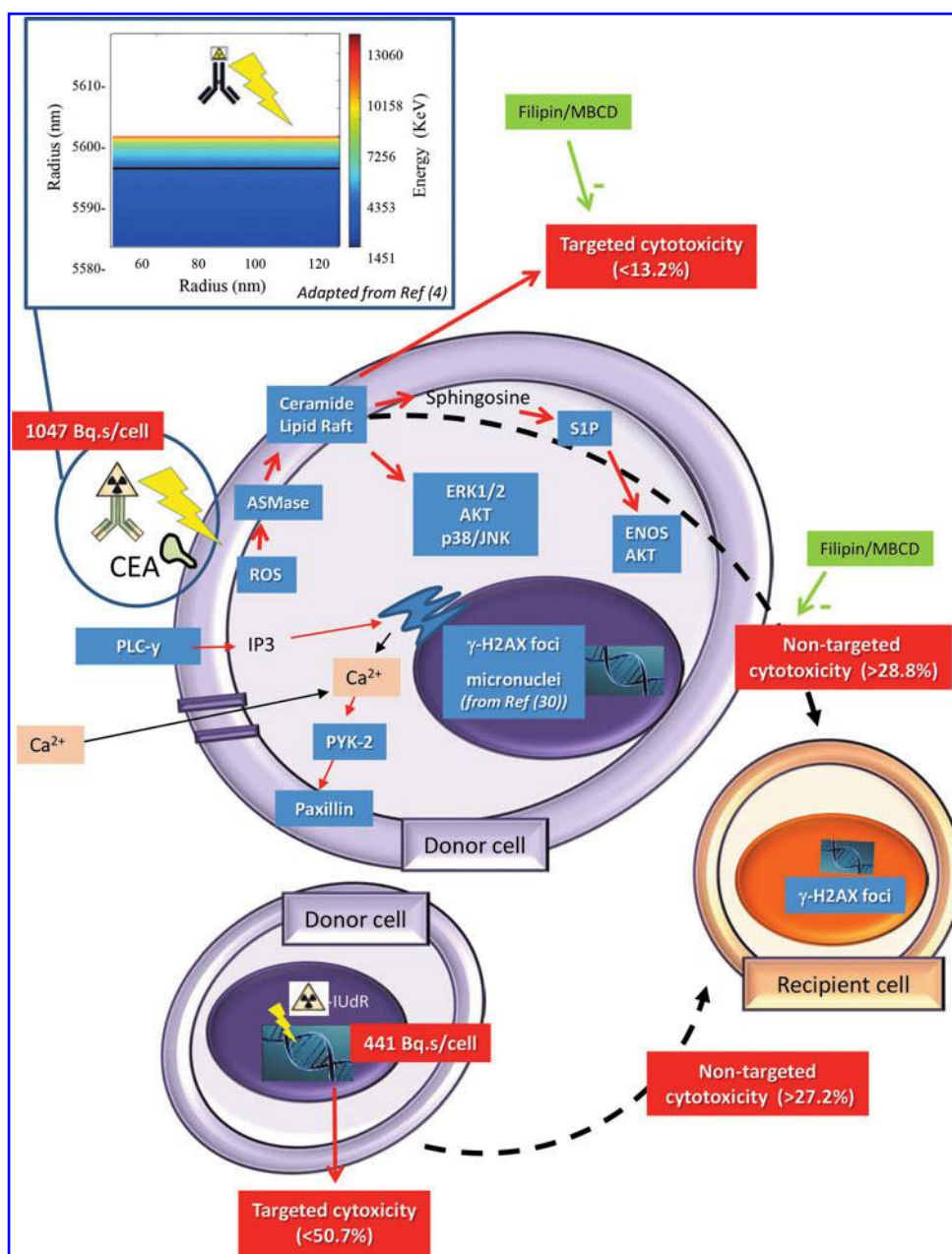
distribution of radioactivity. We observed that radioactivity was mainly localized at the periphery of tumors, whereas DNA DSBs were homogeneously distributed throughout the tumor (Figs. 8B and 9A).

A lower DSB induction was detected after ¹²⁵I-PX mAb treatment, despite the higher nonspecific uptake of radioactivity, for some of the tumors, compared to anti-CEA ¹²⁵I-mAb. These data indicate that the DSBs observed after treatment with anti-CEA ¹²⁵I-mAb were not due to nonspecific irradiation. Indeed, we analyzed ¹²⁵I-PX mAb-treated tumors showing high tumor uptake to be able to exclude the possibility that DNA DSBs measured in the center of the tumor were caused by nonspecific irradiation of ¹²⁵I (mainly soft X-rays and electrons) from the tumor periphery to the center. We could also exclude any contribution from blood circulating ¹²⁵I-mAbs in mouse. As the major contribution to

the absorbed dose from ¹²⁵I is due to Auger electrons, radioactivity distribution may be considered to be indicative of the distribution of the absorbed dose. The reason for the observed higher uptake in some areas of tumor of ¹²⁵I-PX mAb-treated mice compared with those treated with ¹²⁵I-anti-CEA mAb (especially the center) is unclear.

It could be that while the nonspecific antibody is able to freely diffuse to the center of the tumor, the CEA binding antibody binds to receptors, and the first of those encountered would be in the periphery. Unless these receptors in the periphery become saturated, substantial penetration of further unbound antibody molecules would be prevented. Notwithstanding this effect, whatever the distribution of radioactivity, we have previously shown that ¹²⁵I-PX mAb does not have a therapeutic effect *in vivo* (53). Accordingly, our results indicate that DNA DSB formation did not correlate with

FIG. 10. Schematic of the mechanisms involved in RIT using ^{125}I -mAbs. ^{125}I -mAbs targeting the cell membrane deliver high and localized energy at the cell surface. ASMase is activated by ROS produced by radiation energy deposition. ASMase catalyzes sphingomyelin hydrolysis to ceramide and phosphorylcholine. Ceramide modifies the cell membrane biophysical properties and participates in the coalescence of sphingolipid- and cholesterol-enriched domains (called lipid rafts) into large ceramide-enriched platforms, leading to cell membrane receptor reorganization and activation of the ERK1/2, AKT, p38/JNK signaling pathways, and their downstream targets. Activation of phospholipase C- γ and of Ca^{2+} -dependent PYK-2 and paxillin is also observed. Lipid raft-dependent radiation-induced nontargeted effects, including cytotoxicity and γH2AX formation, are observed in neighboring cells, whatever the localization of ^{125}I (cell surface or nucleus) and independently of the decay number (1047 Bq·s for ^{125}I -mAbs and 441 Bq·s for ^{125}I -UdR). Nontargeted effects are strongly reduced by filipin or MBCD. ^{125}I -UdR, 5-[(125)I] iodo-2'-deoxyuridine; PLC- γ , phospholipase C- γ ; PYK-2, proline-rich tyrosine kinase 2; ROS, reactive oxygen species. To see this illustration in color, the reader is referred to the web version of this article at www.liebertpub.com/ars



the absorbed dose and that DNA damage occurred to a similar extent both within and beyond the range of the ^{125}I Auger electrons. In a similar approach using ^{212}Pb -mAbs for treating A-431_{CEA} tumor xenografts, we also observed that distribution of DNA damage and induction of abnormal mitosis do not correlate with tumor absorbed dose, a phenomenon not observed with ^{212}Pb -PX nonspecific mAb (data not shown). These data support the involvement, *in vivo*, of nontargeted effects during ^{125}I -mAb RIT, but this needs to be confirmed in further experiments.

One of the issues raised by our study is related to radiation protection since nonirradiated tissues can show DNA damage and subsequent possible cell death or cell transformation. This may have implications for nuclear medicine where about one atom in two ($^{99\text{m}}\text{Tc}$, ^{123}I , ^{125}I , ^{201}Tl , ^{51}Cr , ^{67}Ga , etc.) emits Auger electrons associated with other particles. It was generally considered that Auger binding DNA, or localized in the

cell nucleus, produces high LET radiation. However, there is no guidance on how to calculate the equivalent dose for these radionuclides. It has been proposed by the American Association of Physicists in Medicine that the component of dose from the Auger electrons for radionuclides bound to DNA should be given a preliminary radiation weighting factor of 10 for deterministic effects and 20 for stochastic effects for nuclear localization while ICRP has recommended considering each situation (isotope and localization) separately (23, 24). The dose equivalent calculated with these weighting factors must be modulated by experimentally determined subcellular distributions of the Auger electron emitters. Our study indicates that the nontargeted effect of Auger electron emitters bound to the cell surface has to be considered.

In conclusion, we have shown that Auger electron emitters, such as ^{125}I , conjugated to mAbs directed against the cancer cell surface can be cytotoxic by a cell oxidative, stress-

mediated nontargeted mechanism involving lipid rafts. This nontargeted effect is comparable to that induced by ^{125}I -UdR concentrated in the nucleus of tumor cells. Compared with ^{125}I -UdR, lower targeted cytotoxicity is expected when using ^{125}I -mAbs, but the induction of nontargeted effects could compensate for the inferior efficacy of non-nuclear targeting. Moreover, ^{125}I -mAbs should also be less toxic toward proliferating normal tissue, thus allowing an increase in the injected activities.

These findings are particularly relevant for targeted therapy in which vectors cannot gain access to every tumor cell. Their extrapolation to targeted alpha radiotherapy, now routinely used in clinical radionuclide therapy, should be evaluated.

Materials and Methods

Cell lines

A-431_{CEA} and SK-OV-3_{CEA} cells were obtained by transfecting A-431 vulvar squamous and SKOV-3 ovarian carcinoma cells (from ATCC, Molsheim, France), respectively, using vectors encoding the CEA. $p53^{+/+}$ HCT116 colon adenocarcinoma cells were obtained from ATCC. The $p53^{-/-}$ HCT116 cell line was a kind gift from Professor Bert Vogelstein. HCT116 cells were grown in RPMI 1640 medium supplemented with 10% (v/v) fetal calf serum (FCS), 2 mM L-glutamine, and antibiotics (0.1 U/ml penicillin and 100 $\mu\text{g}/\text{ml}$ streptomycin) at 37°C in a humidified atmosphere with 5% CO_2 . A-431_{CEA} and SKOV-3_{CEA} cells were grown as described (50). All cell culture reagents were from Life Technologies (Thermo Fisher Scientific, Waltham, MA).

Radiolabeled vectors for cell targeting

To target the cytoplasm, ^{125}I was coupled to the internalizing mouse m225 mAb. ^{125}I -labeled m225 mAb is internalized within the cytoplasm after binding to its receptor (HER1). For cell surface localization, ^{125}I was coupled to the noninternalizing mouse IgG1k mAb 35A7. For the CEA Gold 2 epitope (50), 35A7 is specific. The nonspecific PX antibody was used as a control (irrelevant antibody). PX is an IgG1 mAb purified from mouse myeloma P3-X63 cells (30). The three mAbs were obtained from mouse hybridoma ascites fluids by ammonium sulfate precipitation followed by ion exchange chromatography on DE52 cellulose (Whatman, Balston, United Kingdom).

Antibody radiolabeling was performed according to the IODO-GEN (1,3,4,6-tetrachloro-3 α , 6 α -diphenylglycoluril) (Sigma-Aldrich, St. Louis, MO) method (50). ^{125}I -mAb-specific activity was 370 MBq/mg of protein, and immunoreactivity was 60%–95%. All experiments used ^{125}I -mAb activities ≤ 4 MBq/ml. ^{125}I was targeted to the nucleus using the thymidine base analogue ^{125}I -UdR at a specific activity of 81.4 TBq/mmol. ^{125}I -UdR was purchased from PerkinElmer (Waltham, MA).

RIT, medium transfer, and clonogenic survival of irradiated and nonirradiated cells

$p53^{+/+}$ or $p53^{-/-}$ HCT116, SK-OV-3_{CEA}, and A-431_{CEA} cells were cultured in 6-cm Petri dishes (100–500 cells/dish) with 3 ml of medium. The following day, cells were incubated with ^{125}I -mAbs at activities ≤ 4 MBq/ml for 48 h (donor cells). For targeting of the nucleus, due to the higher toxicity

of ^{125}I -UdR, between 100 and 1200 $p53^{+/+}$ HCT116 cells were seeded in 6-cm Petri dishes containing 3 ml of medium and exposed, the following day, to ^{125}I -UdR activities of ≤ 20 kBq/ml for 48 h. Culture medium was then removed, and cells were washed twice with 4 ml phosphate buffered saline (PBS). For clonogenic assays, performed as described in (50), fresh medium (3 ml) was added and donor cells were cultured for 12 days. For investigating the nontargeted response, fresh medium (3 ml) was added to donor cells for 2 h and then transferred to dishes in which cells had been seeded the day before (recipient cells: 100–500 cells/6 cm dish). The transferred medium was checked for radioactivity (values were generally very low, comprising between 0.08% and 0.10% of the activity incubated with donor cells). Donor and recipient cells were then grown for 12 days and colonies stained with crystal violet (2.5 g/l in 45:5 30% [v/v] methanol/paraformaldehyde). Colonies containing 50 or more cells were scored, and the surviving fraction was calculated. The toxicity of unlabeled mAbs was assessed using the same experimental conditions.

Drug treatment

To determine the role of mAb internalization in the bystander response, $p53^{+/+}$ HCT116 cells were exposed for 2 days to ^{125}I -mAbs of activity concentration ≤ 4 MBq/ml in the presence of 0.02% (w/v) sodium azide, a drug that blocks mAb transport into the cytoplasm.

The role of cell membrane lipid raft formation in ^{125}I -mAb-induced bystander effects was investigated by coincubating $p53^{+/+}$ HCT116 donor cells with ^{125}I -mAbs and 4 mM MBCD (Sigma-Aldrich) for 6 h or with 2.5 $\mu\text{g}/\text{ml}$ filipin (Sigma-Aldrich) overnight.

The potential role of oxidative stress in the induction of bystander effects was assessed by coincubating $p53^{+/+}$ HCT116 donor cells with ^{125}I -mAbs and 50 μM NAC (Sigma-Aldrich) (for 2 days) or 0.5% DMSO (Sigma-Aldrich) (overnight).

Immunofluorescence analysis of mAb localization, lipid rafts, and γH2AX foci

For immunofluorescence studies, $p53^{+/+}$ HCT116 cells were plated on 12-mm glass coverslips in culture dishes. They were fixed in 3.7% (v/v) formaldehyde and then permeabilized in 0.1% (v/v) Triton X-100 for 15 min followed by incubation with 1% (v/v) PBS/bovine serum albumin (BSA) for 1 h. To confirm the mAb localization, an Alexa-488-conjugated anti-mouse secondary mAb was used at a dilution of 1:200 (Invitrogen, Saint Aubin, France). F-actin was stained with conjugated phalloidin (1:5000; Sigma-Aldrich), and nuclei with 0.1 $\mu\text{g}/\text{ml}$ Hoechst (Sigma-Aldrich). To visualize lipid rafts, $p53^{+/+}$ HCT116 cells were incubated with Alexa-488-conjugated cholera toxin (Sigma-Aldrich) at a dilution of 1:1000. γH2AX foci were quantified in $p53^{+/+}$ HCT116 cells after exposure to ^{125}I -mAbs for 2 days according to previously described methodology (48). For immunofluorescent colocalization of ceramide and apoptosis marker, cells were incubated with anti-ceramide 15B4 antibody at dilution 1:10 (Alexis Biochemicals, Heidelberg, Germany) for 1 h at 37°C followed by three PBS washing steps and incubation with PE-conjugated goat anti-mouse IgM at a dilution of 1:200 (Jackson Immuno Research, Baltimore, PA) and annexin V conjugated with FITC dilution

1:100 (Beckman Coulter, Marseille, France). Coverslips were then mounted in Mowiol® (Sigma-Aldrich), and images recorded using a 63× or 100×NA objective and a Leica (Leica Microsystems, Wetzlar, Germany) inverted microscope.

Proteome array, subcellular fractionation, and Western blotting

The Human Phospho-Kinase array (Proteome Profiler Array; R&D Systems, Minneapolis, MN) was used to detect the relative phosphorylation levels of 46 kinases in $p53^{+/+}$ HCT116 cellular extracts according to the manufacturer's protocol. To confirm the localization of the targeting mAbs, a subcellular protein fractionation kit (Thermo Scientific) was used according to the manufacturer's protocol. For Western blotting, membrane and cytosolic protein fractions and total lysates (40 μg of each) from $p53^{+/+}$ HCT116 cells and A-431_{CEA} were separated by sodium dodecyl sulfate polyacrylamide gel electrophoresis and electrotransferred to polyvinylidene difluoride membranes (Amersham Pharmacia Biotech, Uppsala, Sweden). Membranes were incubated with the 35A7 (anti-CEA), m225 (anti-EGFR), sodium/potassium ATPase (1:1000; Abcam, Cambridge, United Kingdom), and anti-tubulin (1:10,000; Abcam) primary antibodies that were then detected with horseradish peroxidase-conjugated goat anti-mouse or anti-rabbit (Sigma-Aldrich) secondary antibodies. p-ERK, p-AKT, and p-p38 were detected by primary anti-p-ERK, anti-p-AKT, and anti-p-p38 antibodies (Cell Signaling Technology, Danvers, MA) followed by incubation with horseradish peroxidase-conjugated goat anti-mouse or anti-rabbit (Sigma-Aldrich) secondary antibodies. Proteins were detected by enhanced chemoluminescence (ECL) using the ECL detection system from Amersham Biosciences (Saclay, France).

Ceramide measurement by flow cytometric analysis

Ceramide levels present in the cell membrane of $p53^{+/+}$ HCT116 cells were assessed by flow cytometry. Cells were treated with unlabeled mAbs (20 $\mu\text{g}/\text{ml}$) or ^{125}I -mAbs (4 MBq/ml) at 37°C for 1 h. After three washes, cells were fixed in 3.7% (v/v) paraformaldehyde for 15 min. Then, cells were washed three times in PBS buffer and incubated with the anti-ceramide 15B4 mAb at a dilution of 1:50 (Alexis Biochemicals) at 37°C for 1 h. After three washes in PBS—2% FCS, cells were incubated with PE-conjugated goat anti-mouse IgM at a dilution of 1:100 (Jackson ImmunoResearch) in the dark for 1 h. Cells were then washed three times and suspended in PBS for analysis using a Muse flow cytometer (Merck Millipore, Fullerton, CA). The y axis corresponds to the total number of analyzed cells (arbitrary units), while the x axis represents the fluorescence signal intensity (PE-conjugated goat mAb anti-ceramide 15B4 mAb). The numbers provided in the red boxes correspond to the proportion of ceramide-positive cells within the total population of cells compared with the nontreated control.

Inhibitors of MAPK pathways and chelation of extracellular Ca^{2+}

To confirm the involvement of MAPK proteins, including AKT, ERK1/2, p38, and JNK on final survival outcome, HCT116 donor cells were incubated for 48 h with ^{125}I -anti-

CEA mAb in the presence of 1 μM of PI3K inhibitor (ZSTK474), and indirectly of downstream AKT signaling pathway, 1 μM of MEK1/2 inhibitor (U0126), and indirectly of downstream ERK1/2 signaling pathway, 10 μM of SP600125 (JNK inhibitor), 10 μM of SB203580 (p38 inhibitor), or 5 mM EGTA (to chelate extracellular Ca^{2+} ions). Donor cells were preincubated with inhibitors 1 h before addition of ^{125}I -mAbs. After 48 h, medium was removed and standard medium transfer protocol was followed as previously described. Clonogenic survival of both donor and recipient cells was measured. The efficacy of ZSTK474 and of U0126 in inhibiting AKT and ERK1/2 was confirmed by Western blotting (Supplementary Fig. S3B, right panel).

Measurement of ASMase activity

ASMase activity in whole cell lysates of $p53^{+/+}$ HCT116 cells exposed to ^{125}I -mAbs (0–4 MBq/ml) for 2 days was measured using the Amplex Red Sphingomyelinase Assay Kit (Molecular Probes, Saint Aubin, France). The ASMase activity of experimental samples and positive control was calculated as a percentage of the ASMase activity of the negative control.

Measurement of S1P concentration

The level of S1P was determined in $p53^{+/+}$ HCT116 cells exposed to ^{125}I -mAbs (4 MBq/ml) for 2 days using the Sphingosine 1 Phosphate Assay Kit according to the manufacturer's protocol (Echelon Biosciences, Salt Lake City, UT).

Animal model

Swiss nude mice (7-week-old females) from Charles River were acclimated for 1 week before experimental use. They were housed at 22°C and 55% humidity with a light–dark cycle of 12 h. Food and water were available *ad libitum*. Body weight was determined weekly, and the mice were clinically examined throughout the study. All animal experiments were performed in compliance with the guidelines of the French government and the INSERM standards for experimental animal studies (agreement B34-172–27).

In vivo experiments

Swiss nude mice (7-week-old females) from Charles River were xenografted intraperitoneally (i.p.) with 1.5×10^6 A-431_{CEA} cells suspended in 0.3 ml PBS. The A-431_{CEA} cell line was chosen for *in vivo* ^{125}I experiments because it expresses high levels of CEA receptors (compared with HCT116 cells), which enables treatment with a tumoricidal dose.

RIT experiments with or without MBCD. For these experiments, 32 mice were divided in four groups ($n=8/\text{each}$) that were treated as follows: (i) two i.p. injections of NaCl at day 8 and 11 postgraft, (ii) two i.p. injections of anti-CEA mAb (100 μg) at day 8 and 11, (iii) two i.p. injections of 37 MBq of ^{125}I -anti-CEA mAb at day 8 and 11, (iv) daily i.p. injections of 300 mg/kg MBCD from day 6 to 15 postgraft, and (v) daily i.p. injections of MBCD from day 6 to 15 and two injections of 37 MBq of ^{125}I -anti-CEA mAb at day 8 and 11 postgraft. At day 30 postgraft, mice were sacrificed, tumors collected, and the total tumor mass was determined.

For this purpose, length, width, and depth of each tumor nodule was measured and used for calculating the nodule volume and a density of 1.05 g/cm³ was used to determine each nodule mass. The average total tumor mass for each mouse was calculated by summing up the mass value of each nodule.

Digital autoradiography and immunohistochemical detection of 53BP1. Ten days postgraft, eight mice were injected i.p. with 37 MBq of ¹²⁵I-PX or of ¹²⁵I-anti-CEA mAbs. Four and 24 h later, mice were anesthetized, bled, and dissected. Tumors were collected and frozen after inclusion in optimal cutting temperature embedding matrix. Two consecutive 10 μ m-thick frozen sections were analyzed by digital autoradiography (DAR) or by immunohistochemical analysis. DAR acquisition was performed using a Beta Imager 2000 instrument (Biospace, Paris, France) over 24 h and analyzed using M3vision software to determine the radioactivity distribution. Immunofluorescence analysis of 53BP1 expression was performed to assess DNA DSB formation. Frozen sections were rehydrated in PBS for 10 min, fixed in 3.7% (v/v) formaldehyde, and then permeabilized in 0.5% (v/v) Triton X-100 for 15 min followed by incubation with 10% (v/v) PBS/BSA for 1 h. Sections were incubated at 37°C with an anti-53BP1 mAb (1:400) for 1 h followed by incubation with an Alexa-594-conjugated anti-rabbit secondary antibody (1:500; Invitrogen). Nuclei were stained with 0.1 μ g/ml Hoechst. The distribution of 53BP1 foci was determined in 100 cells in two relevant areas of representative tumors. All animal experiments were performed in compliance with the guidelines of the French government and the INSERM standards for experimental animal studies (agreement B34-172-27). They were approved by the local ethic committee of “Institut de Recherche en Cancérologie de Montpellier” (IRCM/INSERM) and by the Ethic Committee of Languedoc Roussillon (CEEA LR France No. 36) for animal experiments under the number 1056.

Statistical analysis

All *in vitro* data were obtained from four independent experiments in triplicate. Data were described using mean and standard deviation. Analysis of variance was used for multigroup comparisons (significance level set at $\alpha=0.05$). Pairwise comparisons were performed using the Student's *t* test, and to control for multiple testing, the significance threshold was set at 0.013 in these comparisons.

Data were analyzed using Stata software, version 13 (StataCorp, College Station, TX).

Acknowledgments

This work was supported by Action Nu1.1 of Plan Cancer 2009–2013 (ASC 13038FSA), by the French National Research Agency under the program “Investissements d’avenir” Grant agreement LabEx MAbImprove: ANR-10-LABX-53, Grant INCa-DGOS-Inserm 6045, and the People Programme (Marie Curie Actions) of the European Union’s Seventh Framework Programme (FP7/2007–2013) under REA grant agreement No. 608765 and Marie Curie WHRI Academy COFUND programme.

Author Disclosure Statement

No competing financial interests exist.

References

1. Anthony LB, *et al.* Indium-111-pentetreotide prolongs survival in gastroenteropancreatic malignancies. *Semin Nucl Med* 32: 123–132, 2002.
2. Azzam EI, de Toledo SM, and Little JB. Oxidative metabolism, gap junctions and the ionizing radiation-induced bystander effect. *Oncogene* 22: 7050–7057, 2003.
3. Azzam EI, *et al.* Oxidative metabolism modulates signal transduction and micronucleus formation in bystander cells from alpha-particle-irradiated normal human fibroblast cultures. *Cancer Res* 62: 5436–5442, 2002.
4. Belyakov OV, *et al.* Delayed lethality, apoptosis and micronucleus formation in human fibroblasts irradiated with X-rays or alpha-particles. *Int J Radiat Biol* 75: 985–993, 1999.
5. Bishayee A, Rao DV, and Howell RW. Evidence for pronounced bystander effects caused by nonuniform distributions of radioactivity using a novel three-dimensional tissue culture model. *Radiat Res* 152: 88–97, 1999.
6. Boyd M, *et al.* Radiation-induced biologic bystander effect elicited *in vitro* by targeted radiopharmaceuticals labeled with alpha-, beta-, and auger electron-emitting radionuclides. *J Nucl Med* 47: 1007–1015, 2006.
7. Bradley EW, Chan PC, and Adelstein SJ. The radiotoxicity of iodine-125 in mammalian cells. I. Effects on the survival curve of radioiodine incorporated into DNA. *Radiat Res* 64: 555–563, 1975.
8. Chalfant CE, *et al.* Long chain ceramides activate protein phosphatase-1 and protein phosphatase-2A. Activation is stereospecific and regulated by phosphatidic acid. *J Biol Chem* 274: 20313–20317, 1999.
9. Chen P, *et al.* Antitumor effects and normal tissue toxicity of ¹¹¹In-labeled epidermal growth factor administered to athymic mice bearing epidermal growth factor receptor-positive human breast cancer xenografts. *J Nucl Med* 44: 1469–1478, 2003.
10. Chouin N, *et al.* Evidence of extranuclear cell sensitivity to alpha-particle radiation using a microdosimetric model. II. Application of the microdosimetric model to experimental results. *Radiat Res* 171: 664–673, 2009.
11. Church LD, *et al.* TNFR1-induced sphingomyelinase activation modulates TCR signaling by impairing store-operated Ca²⁺ influx. *J Leukoc Biol* 78: 266–278, 2005.
12. Commerford SL, *et al.* Radiotoxicity of intranuclear ¹²⁵I atoms not bound to DNA. *Int J Radiat Biol Relat Stud Phys Chem Med* 37: 547–554, 1980.
13. Cordes N, *et al.* Human pancreatic tumor cells are sensitized to ionizing radiation by knockdown of caveolin-1. *Oncogene* 26: 6851–6862, 2007.
14. Costantini DL, *et al.* ¹¹¹In-labeled trastuzumab (herceptin) modified with nuclear localization sequences (NLS): an Auger electron-emitting radiotherapeutic agent for HER2/neu-amplified breast cancer. *J Nucl Med* 48: 1357–1368, 2007.
15. Costantini DL, *et al.* Antitumor effects and normal-tissue toxicity of ¹¹¹In-nuclear localization sequence-trastuzumab in athymic mice bearing HER-positive human breast cancer xenografts. *J Nucl Med* 51: 1084–1091, 2010.
16. Delpassand ES, *et al.* Safety and efficacy of radionuclide therapy with high-activity In-111 pentetreotide in patients

- with progressive neuroendocrine tumors. *Cancer Biother Radiopharm* 23: 292–300, 2008.
17. DeSombre ER, *et al.* Therapy of estrogen receptor-positive micrometastases in the peritoneal cavity with Auger electron-emitting estrogens—Theoretical and practical considerations. *Acta Oncol* 39: 659–666, 2000.
 18. Galanis E, *et al.* Phase I trial of sequential administration of raltitrexed (Tomudex) and 5-iodo-2'-deoxyuridine (IdUrd). *Ann Oncol* 12: 701–707, 2001.
 19. Hamada N. Evidence and significance of non-targeted effects of ionizing radiation. *Curr Mol Pharmacol* 4: 78, 2011.
 20. Havaki S, *et al.* The role of oxidative DNA damage in radiation induced bystander effect. *Cancer Lett* 356: 43–51, 2015.
 21. Hehlhans S, Eke I, and Cordes N. Targeting FAK radiosensitizes 3-dimensional grown human HNSCC cells through reduced Akt1 and MEK1/2 signaling. *Int J Radiat Oncol Biol Phys* 83: e669–e676, 2012.
 22. Hofer KG and Hughes WL. Radiotoxicity of intranuclear tritium, 125 iodine and 131 iodine. *Radiat Res* 47: 94–101, 1971.
 23. Humm JL, Howell RW, and Rao DV. Dosimetry of Auger-electron-emitting radionuclides: Report no. 3 of AAPM Nuclear Medicine Task Group No. 6. *Med Phys* 21: 1901–1915, 1994.
 24. ICRP, A.o.t. (Ed). *The 2007 Recommendations of the International Commission on Radiological Protection*. Oxford: Elsevier, Vol. 37, 2007.
 25. Kassis AI. Radiotargeting agents for cancer therapy. *Expert Opin Drug Deliv* 2: 981–991, 2005.
 26. Kassis AI, *et al.* Lethality of Auger electrons from the decay of bromine-77 in the DNA of mammalian cells. *Radiat Res* 90: 362–373, 1982.
 27. Kassis AI, *et al.* Radiotoxicity of an ¹²⁵I-labeled DNA intercalator in mammalian cells. *Radiat Res* 118: 283–294, 1989.
 28. Kassis AI, *et al.* Radiotoxicity of ¹²⁵I in mammalian cells. *Radiat Res* 111: 305–318, 1987.
 29. Kassis AI, Sastry KS, and Adelstein SJ. Kinetics of uptake, retention, and radiotoxicity of ¹²⁵IUDR in mammalian cells: Implications of localized energy deposition by Auger processes. *Radiat Res* 109: 78–89, 1987.
 30. Kohler G, Howe SC, and Milstein C. Fusion between immunoglobulin-secreting and nonsecreting myeloma cell lines. *Eur J Immunol* 6: 292–295, 1976.
 31. Krenning EP, *et al.* The role of radioactive somatostatin and its analogues in the control of tumor growth. *Recent Results Cancer Res* 153: 1–13, 2000.
 32. Lajoie P, *et al.* Caveolin-1 regulation of dynamin-dependent, raft-mediated endocytosis of cholera toxin-B sub-unit occurs independently of caveolae. *J Cell Mol Med* 13: 3218–3225, 2009.
 33. Lehnert BE, Goodwin EH, and Deshpande A. Extracellular factor(s) following exposure to alpha particles can cause sister chromatid exchanges in normal human cells. *Cancer Res* 57: 2164–2171, 1997.
 34. Lev S, *et al.* Protein tyrosine kinase PYK2 involved in Ca(2+)-induced regulation of ion channel and MAP kinase functions. *Nature* 376: 737–745, 1995.
 35. Li L, *et al.* A Phase II study of anti-epidermal growth factor receptor radioimmunotherapy in the treatment of glioblastoma multiforme. *J Neurosurg* 113: 192–198, 2010.
 36. Li PL and Gulbins E. Lipid rafts and redox signaling. *Antioxid Redox Signal* 9: 1411–1415, 2007.
 37. Limouris GS, *et al.* Selective hepatic arterial infusion of In-111-DTPA-Phe1-octreotide in neuroendocrine liver metastases. *Eur J Nucl Med Mol Imaging* 35: 1827–1837, 2008.
 38. Lyng FM, *et al.* The involvement of calcium and MAP kinase signaling pathways in the production of radiation-induced bystander effects. *Radiat Res* 165: 400–409, 2006.
 39. Lyng FM, Seymour CB, and Mothersill C. Initiation of apoptosis in cells exposed to medium from the progeny of irradiated cells: A possible mechanism for bystander-induced genomic instability? *Radiat Res* 157: 365–370, 2002.
 40. Macapinlac HA, *et al.* Pilot clinical trial of 5-[¹²⁵I]iodo-2'-deoxyuridine in the treatment of colorectal cancer metastatic to the liver. *J Nucl Med* 37: 25S–29S, 1996.
 41. Mariani G, *et al.* Tumor targeting in vivo and metabolic fate of 5-[iodine-125]iodo-2'-deoxyuridine following intratumoral injection in patients with colorectal cancer. *J Nucl Med* 34: 1175–1183, 1993.
 42. Mothersill C and Seymour CB. Cell-cell contact during gamma irradiation is not required to induce a bystander effect in normal human keratinocytes: Evidence for release during irradiation of a signal controlling survival into the medium. *Radiat Res* 149: 256–262, 1998.
 43. Nagasawa H, *et al.* Involvement of membrane signaling in the bystander effect in irradiated cells. *Cancer Res* 62: 2531–2534, 2002.
 44. Narayanan PK, Goodwin EH, and Lehnert BE. Alpha particles initiate biological production of superoxide anions and hydrogen peroxide in human cells. *Cancer Res* 57: 3963–3971, 1997.
 45. Oskouian B and Saba JD. Cancer treatment strategies targeting sphingolipid metabolism. *Adv Exp Med Biol* 688: 185–205, 2010.
 46. Paillas S, *et al.* Apoptosis and p53 are not involved in the anti-tumor efficacy of ¹²⁵I-labeled monoclonal antibodies targeting the cell membrane. *Nucl Med Biol* 40: 471–480, 2013.
 47. Patel HH, Murray F, and Insel PA. Caveolae as organizers of pharmacologically relevant signal transduction molecules. *Annu Rev Pharmacol Toxicol* 48: 359–391, 2008.
 48. Piron B, *et al.* DNA damage-centered signaling pathways are effectively activated during low dose-rate Auger radioimmunotherapy. *Nucl Med Biol* 41 Suppl: e75–e83, 2014.
 49. Pomplun E, Booz J, and Charlton DE. A Monte Carlo simulation of Auger cascades. *Radiat Res* 111: 533–552, 1987.
 50. Pouget JP, *et al.* Cell membrane is a more sensitive target than cytoplasm to dense ionization produced by auger electrons. *Radiat Res* 170: 192–200, 2008.
 51. Prise KM and O'Sullivan JM. Radiation-induced bystander signalling in cancer therapy. *Nat Rev Cancer* 9: 351–360, 2009.
 52. Quang TS and Brady LW. Radioimmunotherapy as a novel treatment regimen: ¹²⁵I-labeled monoclonal antibody 425 in the treatment of high-grade brain gliomas. *Int J Radiat Oncol Biol Phys* 58: 972–975, 2004.
 53. Santoro L, *et al.* Noninternalizing monoclonal antibodies are suitable candidates for ¹²⁵I radioimmunotherapy of small-volume peritoneal carcinomatosis. *J Nucl Med* 50: 2033–2041, 2009.
 54. Sastry KS and Rao DV. Dosimetry of low energy electrons. In: *Physics of Nuclear Medicine: Recent Advances*, edited

- by Rao DV, Chandra R, and Graham MC. New York: American Institute of Physics, 1984, pp. 169–208.
55. Sawant SG, *et al.* The bystander effect in radiation oncogenesis: I. Transformation in C3H 10T1/2 cells in vitro can be initiated in the unirradiated neighbors of irradiated cells. *Radiat Res* 155: 397–401, 2001.
 56. Scheel-Toellner D, *et al.* Reactive oxygen species limit neutrophil life span by activating death receptor signaling. *Blood* 104: 2557–2564, 2004.
 57. Singer SJ, and Nicolson GL. The fluid mosaic model of the structure of cell membranes. *Science* 175: 720–731, 1972.
 58. Sisson JC, *et al.* Treatment of neuroblastoma with [¹²⁵I]metaiodobenzylguanidine. *J Nucl Biol Med* 35: 255–259, 1991.
 59. Smith EL and Schuchman EH. The unexpected role of acid sphingomyelinase in cell death and the pathophysiology of common diseases. *FASEB J* 22: 3419–3431, 2008.
 60. Todd DG, *et al.* Ionizing radiation stimulates existing signal transduction pathways involving the activation of epidermal growth factor receptor and ERBB-3, and changes of intracellular calcium in A431 human squamous carcinoma cells. *J Recept Signal Transduct Res* 19: 885–908, 1999.
 61. Valerie K, *et al.* Radiation-induced cell signaling: inside-out and outside-in. *Mol Cancer Ther* 6: 789–801, 2007.
 62. Vallis KA, *et al.* Phase I trial to evaluate the tumor and normal tissue uptake, radiation dosimetry and safety of (111)In-DTPA-human epidermal growth factor in patients with metastatic EGFR-positive breast cancer. *Am J Nucl Med Mol Imaging* 4: 181–192, 2014.
 63. Walicka MA, Adelstein SJ, and Kassis AI. Indirect mechanisms contribute to biological effects produced by decay of DNA-incorporated iodine-125 in mammalian cells in vitro: clonogenic survival. *Radiat Res* 149: 142–146, 1998.
 64. Walicka MA, Adelstein SJ, and Kassis AI. Indirect mechanisms contribute to biological effects produced by decay of DNA-incorporated iodine-125 in mammalian cells in vitro: double-strand breaks. *Radiat Res* 149: 134–141, 1998.
 65. Welt S, *et al.* Phase I/II study of iodine 125-labeled monoclonal antibody A33 in patients with advanced colon cancer. *J Clin Oncol* 14: 1787–1797, 1996.
 66. Xue LY, *et al.* Bystander effect produced by radiolabeled tumor cells in vivo. *Proc Natl Acad Sci U S A* 99: 13765–13770, 2002.
 67. Zhang AY, *et al.* Acid sphingomyelinase and its redox amplification in formation of lipid raft redox signaling platforms in endothelial cells. *Antioxid Redox Signal* 9: 817–828, 2007.
 68. Zhang Y, *et al.* Ceramide-enriched membrane domains—Structure and function. *Biochim Biophys Acta* 1788: 178–183, 2009.

Address correspondence to:

Dr. Jean-Pierre Pouget
 Institut de Recherche en Cancérologie (IRCM)
 INSERM U1194
 208 rue des apothicaires
 34298 Montpellier cedex 5
 France

E-mail: jean-pierre.pouget@inserm.fr

Date of first submission to ARS Central, November 26, 2015; date of final revised submission, May 17, 2016; date of acceptance, May 23, 2016.

Abbreviations Used

53BP1 = p53-binding protein 1
 ASMase = acid sphingomyelinase
 CREB = C-AMP Response Element-binding protein
 DAR = digital autoradiography
 DMSO = dimethyl sulfoxide
 DSB = double-strand break
 ECL = enhanced chemoluminescence
 e-NOS = endothelial nitric oxide synthase
 ERK = extracellular signal-related kinase
 FAK = focal adhesion kinase
 FCS = fetal calf serum
 GSK3 = glycogen synthase kinase 3
 HER1 = Human Epidermal Receptor type 1
¹²³I = iodine 123
¹²⁵I = iodine 125
¹¹¹In = indium 111
 i.p. = intraperitoneally
 IP3 = inositol triphosphate
¹²⁵I-UdR = 5-[(125)I]iodo-2'-deoxyuridine
 JNK = c-Jun N-terminal kinase
 LET = linear energy transfer
 mAb = monoclonal antibody
 MAPK = mitogen-activated protein kinases
 MBCD = methyl-β-cyclodextrin
 MSK = mitogen- and stress-activated protein kinase
 NAC = N-acetyl cysteine
 p70S6K = p70S6 kinase
 PBS = phosphate buffered saline
 PLC-γ = phospholipase C-γ
 PYK-2 = proline-rich tyrosine kinase 2
 RIT = radioimmunotherapy
 RNS = reactive nitrogen species
 ROS = reactive oxygen species
 RSK = 90kDa ribosomal S6 kinase
 S1P = sphingosine-1-phosphate
 STAT1/2/3/4 = signal transducer and activator of transcription 1/2/3/4